hydrogen

MDPI

Article

Coupling PEM Electrolysis and Catalytic Methanation of Biogenic CO_2 in Southern Spain: A Techno-Economic Feasibility Study

Carlos Ortiz [1,2,*], César Martin-Montalvo [1], Sebastián García-Luna [3] and Manuel Antonio Díaz-Pérez [1,2]

[1] Department of Engineering, Universidad Loyola Andalucía, 41704 Dos Hermanas, Spain; cmartinmontalvo@al.uloyola.es (C.M.-M.)
[2] Instituto de Investigación en Energía, Tecnología y Sostenibilidad (LETS), Universidad Loyola Andalucía, 41704 Dos Hermanas, Spain
[3] Decarbonization & CCUS Group, Repsol Technology Laboratory, Industrial Transformation Department, 28935 Móstoles, Spain
* Correspondence: cortiz@uloyola.es

Abstract

Synthetic natural gas (SNG) from renewable hydrogen and captured CO_2 has reached the commercial stage; it is more expensive than fossil gas but may be justified as a renewable fuel for hard-to-decarbonize industry, and its cost depends strongly on how renewable generation, storage and grid electricity are combined. This work reports an hourly techno-economic assessment of a 10 MWe PEM electrolysis and catalytic methanation plant fed with biogenic CO_2 in the Huelva chemical cluster (southwest Spain), built on a rigorous AVEVA Process Simulation model with Xu–Froment kinetics. At design conditions, a two-reactor train converts 98.2% of the CO_2 into 322 kg/h of gas at 95.3 mol% CH_4. Over a year, the base case produces 2140 t of SNG, with 50.8% of the available electricity (LHV) converted into SNG,and a levelized cost of 217.4 €/MWh (2.88 €/kg). Sizing the electrolyzer to the reactor and supplying it with firm grid power lowers the cost to 160.4 €/MWh, or to 178.4 €/MWh with the contract held at 5 MW. These are production costs; whether the plant is profitable depends on the price and support that renewable methane can obtain.

Keywords: CO_2 methanation; Power-to-Gas; PEM electrolysis; e-methane; process modelling; synthetic natural gas (SNG)

Academic Editor: Mihaela Diana Lazar

Received: 30 September 2026
Revised: 29 October 2026
Accepted: 31 October 2026
Published: 10 November 2026

Copyright: © 2026 by the authors. Licensee MDPI, Basel, Switzerland. This article is an open access article distributed under the terms and conditions of the Creative Commons Attribution (CC BY) license.

1. Introduction

Meeting the temperature goals of the Paris Agreement requires reaching net zero CO_2 emissions around mid-century, and the remaining carbon budget requires urgent actions [1]. Electricity is decarbonizing faster than any other energy carrier, but a large part of European final energy demand is still delivered as a combustible gas [2]. The European Union has responded with a policy package that raises the 2030 renewable share to at least 42.5% and that, for the first time, sets binding sub-targets for renewable hydrogen and its derivatives in industry and transport [3].

Synthetic methane, or e-methane, is a green fuel with the potential for large-scale deployment since it can rely on the existing gas distribution network, underground storage facilities and compatible end-use industrial equipment. Hydrogen produced by water

electrolysis with renewable electricity is reacted with captured CO_2 over a catalyst bed to give methane and water according to the Sabatier reaction. The viability of e-methane therefore depends less on the chemistry, which is already mature, than on where the plant is located, how the renewable electricity is integrated and how the by-products are valorized.

The European Biogas Association reported 35 e-methane plants in operation in Europe in 2024, 32 of them fully renewable, with a combined output of 449 GWh in 2023 [4]. Most projects rely on either biological (46%) or catalytic (36%) methanation; 64% have a capacity below 10 GWh, and 53% source their CO_2 from anaerobic digestion [4]. The regulatory frame matters as much as the resource. For synthetic methane to count towards the European renewable targets, it has to qualify as a renewable fuel of non-biological origin, and the delegated act that defines that status sets conditions on additionality and on geographic and temporal correlation between the electricity consumed and the renewable generation claimed [5].

Spain is not yet among the leading countries in e-methane deployment, but its potential is large. The national biogas roadmap sets a minimum production target of 10.41 TWh/year by 2030 [6], and upgrading that biogas to biomethane produces a stream of biogenic CO_2 that is already separated and concentrated but is mostly vented today. Spain also has an abundant solar resource for green hydrogen production [7], with utility-scale photovoltaics already competitive in most of the world (44 USD/MWh) [8]. Its grid is largely decarbonized, with zero-emission sources above 75% of generation and renewables above 55% of the mix [9]. However, its average emission intensity, 125 g CO_2eq/kWh in 2024 [10], is well above the 64.8 g CO_2eq/kWh (18 g CO_2eq/MJ) below which Commission Delegated Regulation (EU) 2023/1184 allows grid electricity to count as fully renewable [5]. A Spanish plant that draws from the grid must therefore rely on renewable power purchase agreements (PPAs) that meet the additionality, temporal correlation and geographic correlation conditions of that regulation.

The present work develops a techno-economic assessment of an e-methane plant in southwest Spain. A constant stream of biogenic CO_2 from a neighbouring biomethane plant is converted into grid-quality methane with hydrogen from PEM electrolysis. The electrolyzer is powered by on-site photovoltaics, a battery and a renewable PPA, and the oxygen and reaction heat are sold within the same industrial cluster. The plant is modelled hour by hour over a full year to obtain the levelized cost of the gas produced.

The technical literature on methanation is well developed. Reviews cover the catalysts, the reactor concepts and the demonstration projects in detail [11–14], and the intrinsic kinetics of nickel-catalysed methanation and water–gas shift established by Xu and Froment [15] remain the reference set for fixed-bed reactor modelling [16–18]. Techno-economic work is more fragmented. Gorre et al. optimized the intermediate hydrogen storage of a power-to-gas plant and showed how strongly the equivalent full-load hours of the methanation section drive the cost of the product [19]. Peters et al. reported methane costs of 3.5–3.9 €/kg for a plant of about 1 t/h with various CO_2 sources [20]. Al-Breiki and Bicer [21] placed the renewable supply inside the system boundary, costing a 10 MW PEM electrolysis and methanation plant powered by 10 MW of photovoltaic electricity in Qatar, but still evaluated it at nominal load over 8000 h per year, without hourly analysis. Barón et al. reported a levelized cost of methane of 3.5 €/kg for sorption-enhanced methanation at 99.9% purity, against 2.4–3.3 €/kg for conventional methanation at 95% purity [22]. Gantenbein et al. compared biological and fluidized-bed chains for grid-ready biomethane [23], and Janke et al. examined an integrated concept at bus-fleet scale [24]. Yilmaz et al., working at European system scale, concluded that power-to-gas becomes economic only along a CO_2 price path reaching 160 €/t by 2050 [25]. At the level of integrated renewable hydrogen systems, recent work has extended the analysis to the water balance, using

electrolyzer and fuel-cell waste heat to desalinate the electrolysis feedwater [26] or to co-produce power and fresh water from low-grade heat [27]. In the plant studied here, the reaction water condensed in the methanation section is recycled to the electrolyzer.

Table 1 summarizes these studies. In the present work, (i) the electrolyzer, the compression trains and the methanation section are represented by off-design correlations derived from a rigorous flowsheet with frozen equipment geometry, so their response to a fluctuating hydrogen supply is part of the result; (ii) the capacities that set the hydrogen supply are optimized together against the levelized cost of the SNG and (iii) the oxygen, steam and surplus CO_2 are valorized at a specific industrial site.

Table 1. Previous techno-economic studies of CO_2 methanation compared with the present work.

Study	Scale; Site	H_2 and Electricity Supply	Time Resolution	Methanation Model	Sized or Optimized
Gorre et al. [19]	1–50 MWe	Electrolysis; spot market, contract, PV or wind	Annual operation	Constant efficiency	H_2 storage, methanation unit
Peters et al. [20]	~950 kg/h CH_4; Germany	Purchased H_2 (5.5 €/kg)	Steady state	Aspen Plus, equilibrium	—
Al-Breiki and Bicer [21]	10 MWe; Qatar	PEM; PV	Nominal, 8000 h/y	Mass and energy balance	—
Barón et al. [22]	200 MWe	Purchased H_2 (6 €/kg)	Steady state	Aspen Plus, kinetic	Reactor size
Gantenbein et al. [23]	1 and 6 MWe; Denmark, Germany	PEM or SOEC; fixed electricity price	Steady state	Kinetic; biological, fluidized bed	—
Janke et al. [24]	3–9 MWe; Sweden	PEM; day-ahead spot market	Hourly	Biological, constant efficiency	Electrolyzer, methanation, CO_2 and CH_4 storage
Chauvy et al. [28]	90 MWe	Wind electrolysis; fixed electricity price	Steady state	Aspen Plus, kinetic, adiabatic	Heat integration
This work	**10 MWe; Spain**	**PEM; PV, battery and grid contract**	**Hourly**	**AVEVA, kinetic; off-design correlations**	**PV, battery, electrolyzer, grid contract, H_2 buffer**

The aim of this work is to establish, with realistic figures, the cost at which an e-methane plant at a specific industrial site would deliver SNG. The site is the Huelva chemical cluster in southwest Spain, where a 10 MWe plant would buy biogenic CO_2 from a neighbouring biomethane upgrading plant, take electricity from a dedicated photovoltaic field backed by a battery and a grid supply contract, and sell oxygen and steam into the cluster. A rigorous flowsheet of the whole chain (PEM electrolysis, hydrogen compression and storage, and two-stage catalytic methanation with Xu–Froment kinetics) was built in AVEVA Process Simulation and solved at design conditions. The process was then run off the design over its operating range and reduced to performance correlations, which drive an hourly model of the complete plant written in Python 3.12. On that basis, the levelized cost of the SNG is derived, its sensitivity to the main assumptions is analysed, and the sizing of the plant is optimized.

2. Process Description and Case Study

The plant converts renewable electricity and biogenic CO_2 into synthetic natural gas. A dedicated photovoltaic field is the primary source of electricity. A lithium-ion battery stores power that would otherwise be curtailed and returns it when the solar output falls short, and a PPA allows a limited amount of grid electricity to be drawn as back-up. Electricity is dispatched in merit order: photovoltaic power first, then the battery, and only

then the grid contract. The contracted power is a design variable, bounded by the capacity available at the grid connection point. It affects both the cost of the product and the share of the hydrogen that depends on grid electricity.

This electricity feeds a proton exchange membrane (PEM) electrolyzer. The oxygen is sold to nearby industry. The hydrogen goes to the methanation reactors or is compressed and held in a pressure vessel. The two storage units do different jobs: the battery shifts electricity within the day, whereas the hydrogen buffer decouples methane production from the solar resource. Their effect on plant performance and cost is analysed in Section 4.

Carbon dioxide is bought already separated from a neighbouring biomethane upgrading plant, which delivers a constant biogenic stream, so the plant needs no capture unit. Hydrogen and CO_2 react over a nickel catalyst in two fixed-bed reactors in series, with the reaction water condensed between the stages and at the outlet. Any CO_2 the reactors cannot take in each hour is compressed and sold. The reaction heat is recovered as saturated steam and sold, and the product gas is dried before injection into the gas grid because its water content at the outlet of the last separator exceeds the dew point allowed by the grid specification [29]. The scale of the plant is set by the CO_2 available, 850 kg/h, which is the stream currently leaving the upgrading plant; the electrolyzer, the photovoltaic field and the storage units are sized around it. The base case uses a 10 MW electrolyzer, with the other capacities listed in Table 2 and optimized in Section 4. Figure 1 shows a simplified process flow diagram; the detailed diagram, with the stream labels used in Table A2, is given in Figure A3 (Appendix A.4).

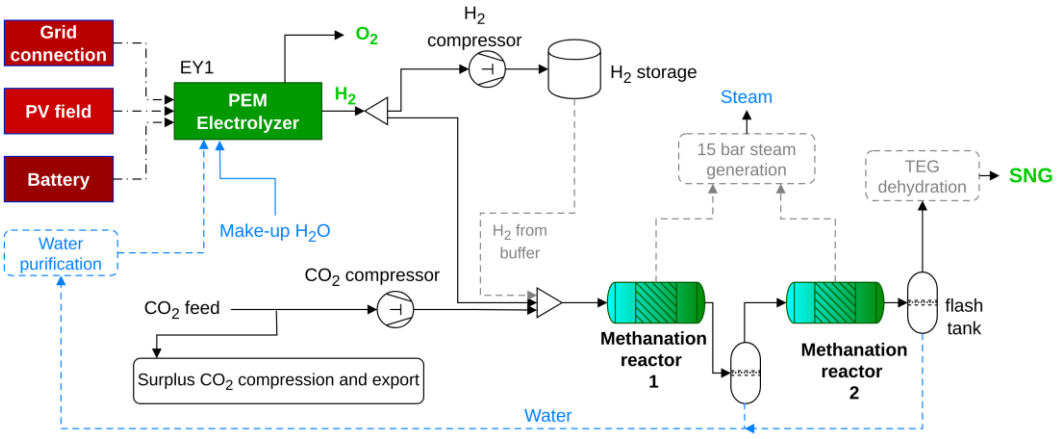

Figure 1. Simplified process flow diagram of the e-methane plant. Solid lines denote units and streams modelled rigorously in AVEVA Process Simulation; dashed lines denote units and streams accounted for only in the hourly dispatch and techno-economic model (mass and energy balances, sizing correlations and costs), without a dedicated flowsheet simulation. Dash-dotted lines denote electrical connections.

The plant would be located in the Huelva chemical cluster, next to Palos de la Frontera, where every stream leaving the plant has a buyer. The oxygen and the 15-bar saturated steam are sold to neighbouring industrial consumers, and the surplus CO_2 is compressed to about 100 bar for industrial use. The dried SNG leaves the plant at about 20 bar, above the 16-bar maximum design pressure of the Spanish distribution networks [30], so it can be injected into the local grid through a pressure-reduction and metering station without a product compressor. The CO_2 is bought at the fence of the upgrading plant, so neither biogas upgrading nor CO_2 separation belongs to this assessment. The grid injection station (fiscal metering, gas analysis, pressure regulation and odorization) and the

delivery infrastructure for oxygen and steam are also outside the battery limits. Table 2 summarizes the base-case capacities.

Table 2. Base-case capacities of the plant.

Item	Value	Unit
Solar resource	TMY (NSRDB)	—
CO_2 supply (fixed, firm)	850 (7446 t/yr)	kg/h
CO_2 stream composition (CO_2/H_2O/CH_4)	97.5/1.5/1.0	mol%
CO_2 delivery pressure/temperature	1.2/30	bar/°C
PV field *	15	MW_{AC}
Battery, energy/power *	10/5	MWh/MW
PEM electrolyzer, nominal power *	10	MW
PEM electrolyzer, operating range	20–110	%
Contracted grid power (PPA) *	5	MW
Hydrogen buffer, capacity *	3000	kg
Hydrogen buffer, pressure range	21–213	bar
Maximum hydrogen flow to methanation	152.3	kg/h
Exported steam, saturated	15	bar
SNG delivery pressure	20.6	bar
Surplus CO_2 export pressure	102.5	bar

* Sizing variables explored in Section 4.

3. Modelling

3.1. Modelling Approach

The plant is modelled at two levels. The first is a rigorous steady-state flowsheet of the process section in AVEVA Process Simulation. It includes the PEM electrolyzer and its water loop; the hydrogen compression train to the buffer; the CO_2 compression train to the reactors; the two methanation reactors with their exchangers, coolers and knock-out drums; and the compression of surplus CO_2 for export. The flowsheet is first solved in design mode, which sizes the equipment for the nominal operating point (Section 3.2), and then converted into an off-design model with the geometry of every unit frozen (Section 3.3). The second level, built on the first, is an hourly model of the complete plant. It dispatches photovoltaic power, battery, grid supply and hydrogen buffer over the 8760 h of a year and represents the process section through correlations fitted to the off-design flowsheet (Section 3.4). The techno-economic model (Section 3.5) uses the annual results of the hourly model.

The hourly model assumes quasi-steady operation: within each hour, the process section is at steady state for the hydrogen available in that hour. The gas residence time in the reactors is a few seconds, far shorter than the time step. The thermal inertia of reactors and exchangers, start-up and shut-down sequences, hot-standby consumption and electrolyzer ramp limits are not represented, so the model tends to overstate the flexibility of the plant in the hours in which it starts or stops. Their frequency is assessed in Section 4.2.

Thermodynamic properties are calculated with the Predictive Soave–Redlich–Kwong (PSRK) equation of state. Its group-contribution mixing rule represents both the hot gas mixture of the reaction section and the vapour–liquid equilibrium of the water-rich condensate in the knock-out drums.

3.2. Design-Point Flowsheet and Main Assumptions

The design point is defined by the full CO_2 stream (850 kg/h) reacting with the hydrogen it can take at the specified H_2/CO_2 ratio, which sets the maximum hydrogen flow to methanation at 152.3 kg/h. At its nominal 10 MW, the electrolyzer produces 202.5 kg/h,

so 50.2 kg/h go to the hydrogen buffer when the solar field runs at full output. Table 3 lists the specifications of the design flowsheet and the main quantities calculated from them. They fix the equipment geometry used off design and, through it, every correlation of the hourly model.

Table 3. Main specifications of the design-point flowsheet.

Parameter	Value	Basis
Feed and thermodynamics		
Thermodynamic package	PSRK	Specified
CO_2 stream flow	850 kg/h	Site data
CO_2 stream composition (CO_2/H_2O/CH_4)	97.5/1.5/1.0 mol%	Site data
CO_2 stream pressure; temperature	1.2 bar; 30 °C	Site data
PEM electrolyzer (EY1)		
Nominal power	10 MW	Specified
Operating range	20–110% of nominal	Specified
Stacks × cells per stack; active area per cell	10 × 120; 0.302 m²	Specified
Membrane	Nafion 117, 0.178 mm	Specified
Membrane water content, λ	14	Specified
Temperature; cathode/anode pressure	80 °C; 21.4/21.5 bar	Specified
Current density (nominal load)	1.49 A/cm²	Calculated
Cell voltage (nominal load)	1.851 V	Calculated
Faraday efficiency (nominal load)	0.997	Calculated
H_2/O_2 production (nominal load)	202.5/1609 kg/h	Calculated
H_2 to methanation (design point)	152.3 kg/h	Design basis
Specific consumption (nominal load)	49.4 kWh/kg H_2	Calculated
Stack cooling duty, not recovered	1.94 MW	Calculated
Hydrogen compression and storage (K1, K2, E2, E3)		
H_2 to buffer (design point)	50.2 kg/h	Design basis
H_2 buffer capacity; pressure range	3000 kg; 21–213 bar	Specified
Compressors	Reciprocating, 2 stages, intercooled	Specified
Pressure ratio per stage	3.2	Specified
Discharge pressure	214 bar	Calculated
Isentropic efficiency	0.80	Specified
Speed; stroke; mean piston speed	675 rpm; 0.20 m; 4.5 m/s	Specified
Cylinder bore K1/K2	79.9/43.1 mm	Calculated
Intercooler area E2/E3	2.41/1.63 m²	Calculated
Shaft power (nominal load)	69.84 kW	Calculated
CO_2 compression to methanation (K3, K4, E1)		
Compressors	Reciprocating, 2 stages, intercooled	Specified
Pressure ratio per stage	4.2	Specified
Discharge pressure	20.9 bar	Specified
Isentropic efficiency; speed; stroke	0.80; 675 rpm; 0.20 m	Specified
Cylinder bore K3/K4	277.9/137.0 mm	Calculated
Intercooler area E1	10.9 m²	Calculated
Shaft power (nominal load)	58.9 kW (249.6 kJ/kg)	Calculated
Surplus CO_2 export (separate flowsheet)		
Compressors	Reciprocating, 3 stages, intercooled	Specified
Discharge pressure	102.5 bar	Specified

Shaft power (nominal load)	88.6 kW (375.1 kJ/kg)	Calculated
Methanation reactors (R1, R2)		
H_2/CO_2 molar ratio at reactor inlet	3.95	Specified
Kinetics	Xu–Froment LHHW	[15]
Catalyst	$Ni/MgAl_2O_4$	Specified
Catalyst particle density	2350 kg/m^3	Specified
Bed void fraction	0.44	Specified
Reactor model (PFR)	Isothermal multitubular	Specified
Reactor pressure drop	0.16 bar	Calculated (Ergun)
R1: tubes × internal diameter × length	50 × 0.10 m × 1.5 m	Specified
R1: catalyst	774.8 kg	Calculated
R1: temperature; pressure	380 °C; 20.85 bar	Specified
R2: tubes × internal diameter × length	20 × 0.10 m × 1.5 m	Specified
R2: catalyst	309.9 kg	Calculated
R2: temperature	400 °C	Specified
R2: pressure	20.69 bar	Calculated
Reaction duty R1/R2	893.6/17.4 kW	Calculated
Heat exchange and separation (E4, E5, E7, E8, V1, V2, V4)		
Feed–effluent exchangers E4/E5 area	28.3/7.9 m^2	Calculated
Effluent coolers E7/E8 area	29.1/5.2 m^2	Calculated
Knock-out drum V2 (D × L), adiabatic	0.15 × 1.5 m	Specified
Knock-out drum V4 (D × L), adiabatic	0.1 × 0.75 m	Specified
Knock-out drum temperature V2/V4	41/32 °C	Calculated
Heat recovery and product conditioning		
Steam raised with the reaction heat	Saturated, 15 bar	Specified
Boiler feed water (BFW)	105 °C, from deaerator	Specified
Specific steam production	1.532 kg/kWh	IAPWS-IF97
Dehydration	TEG absorption; dew point ≤ +2 °C at 70 bar	Specified
CH_4 limit applied at grid injection	>95 mol%	Specified

The electrolyzer stack is modelled in AVEVA Process Simulation as an equivalent electrical circuit, with the open-circuit voltage in series with an activation resistance and the ohmic resistance of the membrane [31] so that the cell voltage is

$$V_{\text{cell}} = V_{\text{oc}} + V_{\text{act}} + V_{\text{ohm}} \quad (1)$$

The open-circuit voltage is the Nernst potential relative to standard pressure,

$$V_{\text{oc}} = V_{\text{rev}}(T) + \frac{RT}{2F} \ln\left[\left(\frac{p_{\text{H}_2}}{P_{\text{std}}}\right)\left(\frac{p_{\text{O}_2}}{P_{\text{std}}}\right)^{0.5}\right] \quad (2)$$

where p_{H2} and p_{O2} are the partial pressures of the product gases in the vapour phase of each chamber, P_{std} = 101.325 kPa, R = 8.314 kJ/(kmol·K) and F = 96,487 C/mol. The cathode delivers dry hydrogen, so p_{H2} is the cathode pressure, while the vapour at the anode is oxygen saturated with water. V_{rev} is the reversible cell voltage, which evaluates the Gibbs free energy of the water-splitting reaction at standard conditions and corrects it with a linear temperature term,

$$V_{\text{rev}} = \frac{\Delta G}{2F} - 9 \times 10^{-4}\,(T - 298), \qquad \Delta G = \Delta H - 298\,\Delta S \quad (3)$$

where ΔH and ΔS are the enthalpy and entropy of reaction, from the standard formation properties of liquid water, hydrogen and oxygen, and T is the stack temperature in K. The

first term is a constant, $\Delta G/(2F)$ = 1.229 V, and the linear term reproduces the measured decrease of the reversible voltage with temperature [32,33].

The activation overpotential is written as a single Butler–Volmer term governed by the charge-transfer coefficient of the anode, which is the controlling electrode,

$$V_{\mathrm{act}} = \frac{RT}{2\,\alpha_{\mathrm{an}}F}\,\mathrm{asinh}\left(\frac{J}{2J_0}\right) \tag{4}$$

$$J_0 = J_{0,\mathrm{std}}\exp\left[-\frac{E_{\mathrm{exc}}}{R}\left(\frac{1}{T}-\frac{1}{T_{\mathrm{std}}}\right)\right] \tag{5}$$

with J the current density on the electrode, α_{an} = 0.7353, $J_{0,std}$ = 1.08 × 10^{-4} A/m^2 and T_{std} = 298.15 K [33]. The ohmic overpotential is the protonic resistance of the membrane,

$$V_{\mathrm{ohm}} = R_{\mathrm{mem}}\,I_{\mathrm{e}}, \qquad R_{\mathrm{mem}} = \frac{\delta_{\mathrm{mem}}}{\sigma_{\mathrm{mem}}\,A_{\mathrm{e}}} \tag{6}$$

$$\sigma_{\mathrm{mem}} = (0.005114\,\lambda - 0.00326)\exp\left[1268\left(\frac{1}{303}-\frac{1}{T}\right)\right] \tag{7}$$

where I_e is the current through one stack, δ_{mem} = 0.178 mm the thickness of the Nafion 117 membrane, A_e the area of one electrode, σ_{mem} the protonic conductivity in S/cm and λ = 14 the water content of the membrane [34]. This value corresponds to a vapour-equilibrated Nafion membrane and is lower than the one that reproduces the stack tested by Espinosa-López et al. [31], $\lambda \approx 22$ (Appendix A.1); it is adopted as a conservative choice that also covers membrane ageing and the electronic resistances not included in the model. Hydrogen production follows Faraday's law,

$$\dot{n}_{\mathrm{H_2}} = \frac{\eta_{\mathrm{F}}\,N_{\mathrm{cell}}\,N_{\mathrm{par}}\,I_{\mathrm{e}}}{2F}, \qquad \dot{n}_{\mathrm{O_2}} = \frac{\dot{n}_{\mathrm{H_2}}}{2} \tag{8}$$

with N_{cell} cells in series per stack, N_{par} stacks in parallel and $J = I_e/A_e$. The Faraday efficiency is not an independent correlation; the electrolyzer takes the specific electricity consumption from a curve against load,

$$P = \dot{m}_{\mathrm{H_2}}\,e(x), \qquad x = \frac{\dot{m}_{\mathrm{H_2}}}{\dot{m}_{\mathrm{H_2,rated}}} \tag{9}$$

where e is the specific consumption in kWh per kilogram of hydrogen and x the fraction of the rated capacity of one stack. The electric power follows from the production, and η_F is the value that closes Equation (8). The resulting polarization curve was checked against experimental data (Appendix A.1).

At the design point, the ten stacks run at their rated capacity, 202.5 kg/h of hydrogen, at 80 °C, 21.5 bar at the anode and 21.4 bar at the cathode. The specific consumption is 49.4 kWh/kg (10.0 MW), 67.5% of the lower heating value of the hydrogen. The cell voltage is 1.851 V (V_{oc} = 1.249 V, V_{act} = 0.388 V, V_{ohm} = 0.214 V) at 1.49 A/cm^2, which gives a voltage efficiency of 80.0% relative to the thermoneutral voltage, and η_F = 0.997. No power conversion loss is charged. The anode is fed with 10% excess water, and the stack rejects 1.94 MW of cooling duty.

Because the cathode operates at 21.4 bar, above the reactor pressure, the hydrogen sent directly to methanation needs no compression; only the surplus sent to the buffer is compressed. The stack cooling duty, at about 80 °C, is too cold to raise process steam and goes to cooling water.

All compressors are reciprocating machines running at 675 rpm with a 0.20 m stroke (piston speed 4.5 m/s), and their cylinder bores were calculated. The geometry does not change the shaft power at the design point, but it matters off design, where the intercoolers

keep their design area. The export train for surplus CO_2 has three stages on a common shaft and handles the part of the stream the reactors do not consume, from zero to the whole stream during maintenance stops.

The two reactors in series are modelled as isothermal plug-flow reactors with the Langmuir–Hinshelwood–Hougen–Watson (LHHW) kinetics of Xu and Froment [15] for steam methane reforming, water–gas shift and overall CO_2 reforming, run in the methanation direction. Over nickel, CO_2 methanation proceeds as a combination of CO methanation and the reverse water–gas shift, both included in this kinetic model, and nickel is the most selective methanation catalyst [18]; oxygenated products such as methanol or formic acid are not formed in significant amounts at these conditions and are not considered. The original parameter set is used, without the activity factor of 1.225 applied in some later studies, and its implementation was validated against an independent integration of the rate equations and compared with the experimental data of Xu and Froment (Appendix A.2). The catalyst is taken as fresh; deactivation enters only as a replacement cost (Section 3.5) [18].

Isothermal operation represents a multitubular reactor cooled by boiling water on the shell side, the usual arrangement to keep a nickel catalyst below its sintering temperature [18]. For R1, the assumption is consistent: removing 894 kW through 23.6 m^2 of tube wall with 15-bar boiling water, at a temperature difference of about 180 K, requires an overall heat-transfer coefficient of about 210 W/(m^2·K), at the low end of the usual range for cooled fixed beds. R2 is a polishing stage that releases only 17 kW. A boiling-water jacket would overcool it, and adiabatic operation would raise its temperature by about 75 K, so it needs a small, controlled heat removal, whose design is outside the scope of this study. Cooled tube-bundle reactors approach isothermal profiles [18] and are in commercial use, as in the Audi e-gas plant in Werlte, whose shell-and-tube reactor is cooled with molten salt [20]. Isothermal reactor models are therefore common in process studies of CO_2 methanation [20,35], alongside adiabatic trains with intercooling [28]. In practice, the heat release makes isothermal operation challenging [20], and cooled fixed beds develop a hot spot near the inlet [36], which can be limited by controlling the coolant temperature [16].

The H_2/CO_2 ratio and the two reactor temperatures were chosen from sweeps of the design flowsheet (Figure 2). The two outlet temperatures were swept between 350 and 420 °C at the design CO_2 flow (Figure 2a). The methane content of the dry product has an interior maximum. At low temperature, the beds are kinetically limited and the methane content falls steeply. Above about 400 °C, the equilibrium shifts back towards the reactants and the reverse water–gas shift gains ground, so the methane content falls again, more gently, while the CO content rises towards the 0.1 mol% limit of the grid specification.

The design pair, 380 °C in R1 and 400 °C in R2, lies inside the region where the product exceeds 95 mol% CH_4, which spans roughly 370–400 °C in R1 and 390–410 °C in R2. A deviation of about ±10 K in either temperature therefore still meets the methane specification.

The feed ratio was swept between 3.85 and 4.15 at the design temperatures (Figure 2b). The optimum is 3.97, and the product stays above 95 mol% CH_4 between 3.926 and 3.999. The curve is asymmetric: an excess of hydrogen reduces the methane content about three times more than the same deficit because four moles of hydrogen react per mole of CO_2 and the unreacted hydrogen stays in the product. The design value of 3.95 was therefore placed on the lean side of the optimum.

Between the reactors, the R1 effluent is cooled in the feed–effluent exchanger E4 and in E7, and the condensed water is removed in drum V2. The gas is reheated in E5 against the R2 effluent before entering R2, and the final cooler E8 and drum V4 remove the

remaining water. Removing water between the stages lets R2 push the conversion beyond the equilibrium of a single reactor. The gas leaving V4 contains 95.30 mol% CH_4, 2.58 mol% H_2, 1.75 mol% CO_2, 0.32 mol% H_2O and 0.06 mol% CO, with a lower heating value of 47.63 MJ/kg. It meets the CO_2 limit of the Spanish gas system specification [29] and the 95 mol% methane threshold. Its hydrogen content exceeds the general limit of 2 mol% but is within the conditional limit of 5 mol% at the injection point, which requires the approval of the system operator [29]. Its water content, about 3200 ppmv, exceeds the dew-point specification (+2 °C at 70 bar), so a triethylene glycol (TEG) dehydration unit is placed after V4. The unit is not simulated; its cost is scaled from a recent assessment of an SNG plant designed for the same specification [37], and its reboiler duty, about 2 kW_{th}, is covered by the reaction heat.

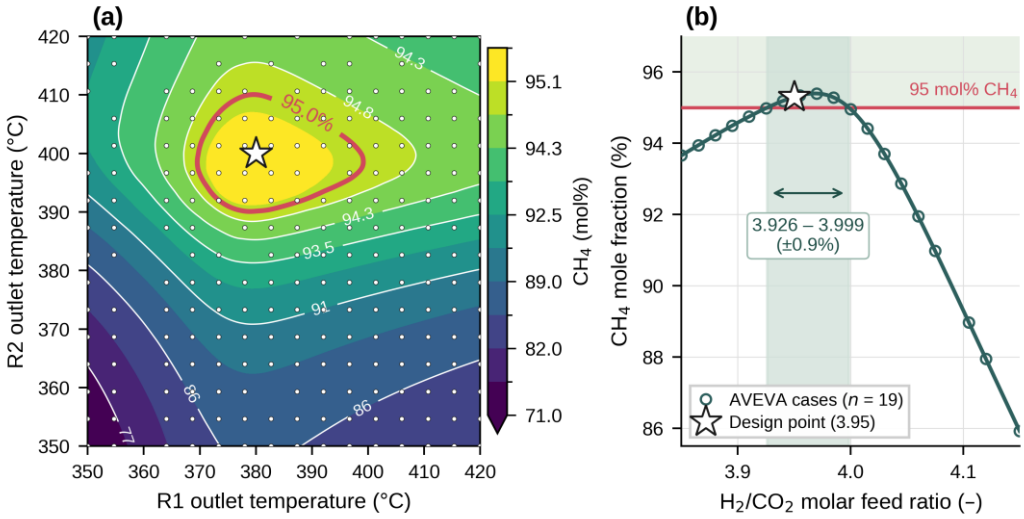

Figure 2. (**a**) CH_4 mole fraction of the dry product as a function of the R1 and R2 outlet temperatures. (**b**) Effect of the H_2/CO_2 molar feed ratio at the design temperatures; the shaded band is the range over which the product stays above 95 mol% CH_4.

The reaction heat is recovered as saturated steam at 15 bar from boiler feed water at 105 °C, which gives 1.532 kg of steam per kWh of heat. The boiling-water circuit, drum and feed pump are not costed, so the steam credit is slightly optimistic.

3.3. Off-Design Characterization and Performance Correlations

The hourly model uses a surrogate of the design flowsheet: algebraic correlations fitted to its converged off-design solutions. They keep the effect of the PSRK equation of state, the reactor kinetics and the frozen equipment geometry, which an annual balance with constant efficiencies would lose.

In the off-design model, the geometry computed at the design point is frozen (exchanger areas, drum dimensions, number and length of tubes, catalyst mass and compressor cylinders), and the reactor outlet temperatures and the reactor inlet pressure are held at their design values. The CO_2 fed to methanation follows the hydrogen available, and the rest of the stream goes to export. Each output of the methanation section is then a function of the hydrogen flow alone, each output of the electrolyzer a function of its power alone, and the power of each compression train a function of its mass flow alone. The hydrogen train is the exception since its discharge pressure follows the buffer. Each correlation was obtained by converging the flowsheet at a series of points across the operating range and fitting a polynomial to the results.

In each compression train, the first stage has a fixed suction state, and its power is linear in mass flow. The following stages are not: as the flow rises, the fixed-area intercoolers lose effectiveness (from 96.6% to 89.2% in the CO_2 train to methanation between 100 and 1000 kg/h), the next stage receives hotter gas and its specific work increases. The two CO_2 trains are therefore described by quadratic functions of mass flow, fitted on dedicated off-design flowsheets at fixed compressor speed. In the integrated flowsheet, the speed is trimmed to the flow, which lowers the duty of the train to methanation by 2.4% at full flow.

The complete set, with coefficients, ranges and coefficients of determination, is given in Table A1 (Appendix A.3); all fits have $R^2 \geq 0.9988$. Figure 3 shows three features of the set that the coefficients alone do not convey.

First, the specific consumption of the electrolyzer is not monotonic in load (Figure 3a), so the fit depends on the operating range considered. The electrolyzer is not operated below 20% of its nominal power (Section 3.4), as is usual for industrial PEM units, and over the resulting range of 2 to 11 MW, a quadratic reproduces the 101 converged cases within 0.4%. A wider range down to zero load, which industrial equipment does not reach, would only have required a higher-order polynomial. Because the correlation is fitted at one electrolyzer size, it is applied in normalized form, so that the nominal power can be varied without leaving its range of validity:

$$\dot{m}_{H_2}(P;\, P_{nom}) = s\, f\left(\frac{P}{s}\right), \qquad s = \frac{P_{nom}}{P_{ref}}, \qquad P_{ref} = 10\ \text{MW} \tag{10}$$

where f is the quadratic of Table A1. The scaling is exact for this equipment: a larger stack adds units in parallel at the same current density and cell area, so the specific consumption depends on the fractional load alone, and the fitted range, 0.20 to 1.10 of nominal power, coincides with the operating window at any size.

Second, the composition of the product barely depends on load (Figure 3b): between 7% and 100% of the nominal CO_2 feed, the methane content changes by less than 0.1 percentage points since the H_2/CO_2 ratio is kept close to its design value. Third, the power of the hydrogen train depends on both flow and buffer pressure (Figure 3c) because the discharge pressure follows the inventory of the buffer, which fills and empties within the day. Its correlation is proportional to the flow and reproduces the design flowsheet within 0.2%.

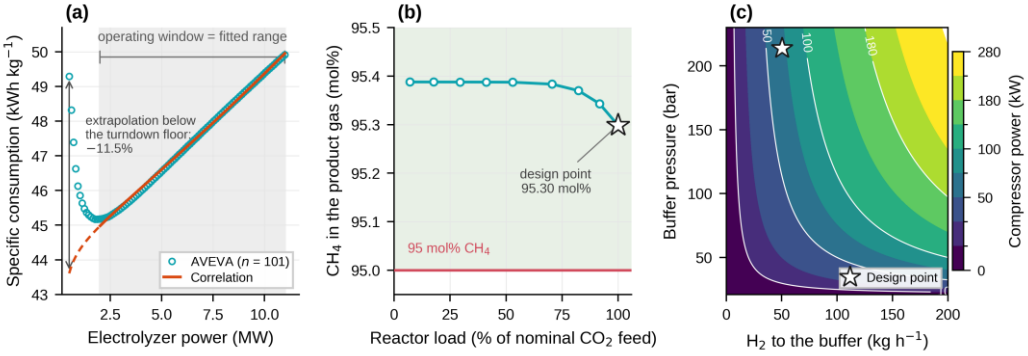

Figure 3. Off-design performance (coefficients in Table A1). (**a**) Specific electricity consumption of the electrolyzer against power. Dashed lines represent the values of the correlation out of the operating window. (**b**) CH_4 content of the product gas against reactor load. (**c**) Power of the hydrogen compression train against the flow sent to the buffer and the buffer pressure.

3.4. Hourly Plant Model

The solar resource is the hourly output of a 1 MW reference plant at Palos de la Frontera (37.21° N, 6.90° W), simulated with NREL's System Advisor Model [38] on a typical meteorological year [39]. The array uses ZNSHINE ZXM7-SHLDD144-555/M modules, fixed-tilt and south-facing, with irradiance, DC and AC losses of 5%, 4.4% and 1%, respectively.

The reference plant delivers 2266 kWh/y per kilowatt of AC capacity, a capacity factor of 25.9%. The hourly series is normalized by the rated power and scaled linearly to the installed capacity of each case, which ignores any change in the loss chain with plant size. All photovoltaic capacities in this work refer to this AC rating.

Figure 4 shows the structure of the resource. Daily generation is regular (Figure 4a), but the seasonal contrast is large (Figure 4b): the best month delivers about twice as much as the worst. Both storage devices work on a daily cycle (the 3000 kg buffer holds about 20 h of reactor feed), so the winter deficit cannot be covered with summer surplus and has to be met by the grid contract or accepted as lost production.

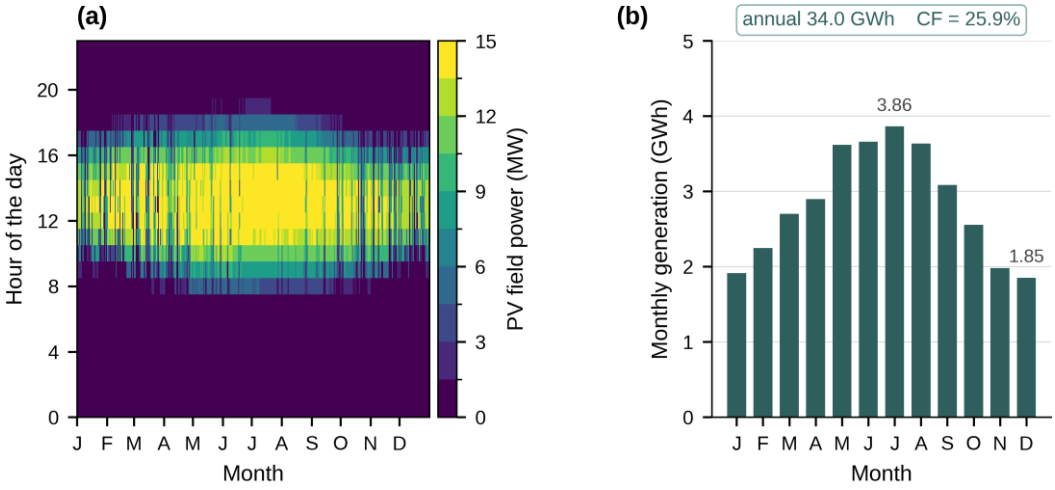

Figure 4. Photovoltaic output of the 15 MW field of the base case at beginning of life, for a typical meteorological year at Palos de la Frontera. (**a**) Hourly power over the year; (**b**) monthly generation.

The merit order of Section 2 is resolved hour by hour. Three powers define the operation of the electrolyzer: the 2 MW turndown floor, the 11 MW ceiling P_{max}, and the power P_t = 7.28 MW at which it produces the 152.3 kg/h of hydrogen the reactors can take (Table A1). Below P_t, the reactors are short of hydrogen; above it, the extra hydrogen goes to the buffer. In each hour, the electrolyzer takes the photovoltaic power available, P_{PV}, and the battery discharges to close the gap up to P_t, within the power B allowed by its state of charge and converter:

$$P_{el} = \min\{P_{max},\ \max[P_{PV},\ \min(P_t,\ P_{PV} + B)]\} \quad (11)$$

The battery can lift the electrolyzer up to P_t but never displaces the photovoltaic power, and the outer minimum applies the ceiling. If the result is below the 2 MW floor, the electrolyzer is shut down for that hour and the battery is not discharged. The photovoltaic power that the electrolyzer does not take charges the battery within its power and state-of-charge limits; the rest is curtailed and sold to the grid up to the rating of the connection.

The battery is not used above P_t because that hydrogen would have to be compressed into the buffer. Stored in the battery and used in a later hour, the same energy produces hydrogen that goes directly to the reactors.

The grid contract is activated when the hydrogen that the photovoltaic power, battery and buffer can deliver in the hour falls below 50% of the reactor capacity. It stays active until that availability recovers to 100% and for at least 4 h. While it is active, the electrolyzer takes the photovoltaic power plus the contracted power, subject to the turndown floor. This rule gives priority to the continuous operation of the reactors and represents the simple and realistic operation of the plant. Because the grid price is flat, its merit order is also the cost order. The optimal designs of Section 4.4 are optimal for this rule; other energy management strategies are outside the scope of this work.

The battery is a 10 MWh, 5 MW lithium-ion system operated between 15 and 95% of its remaining capacity. Its charge and discharge efficiencies fall linearly with the C rate,

$$\eta_{\mathrm{c}} = \max\left[\eta_{\min},\ \eta_0 - k_\eta \frac{P_{\mathrm{c}}}{E}\right], \qquad \eta_{\mathrm{d}} = \max\left[\eta_{\min},\ \eta_0 - k_\eta \frac{P_{\mathrm{d}}}{E}\right] \tag{12}$$

with $\eta_0 = 0.96$, $k_\eta = 0.03$ h, $\eta_{\min} = 0.75$ and E the nominal energy capacity. The state of charge is integrated hourly. Capacity fade follows the System Advisor Model [38], taking the larger of a cycling term (0.008% per equivalent full cycle) and a calendar term (2% per year). With 174 equivalent full cycles a year in the base case, the calendar term dominates, and the pack reaches its 80% end-of-life capacity after ten years, so it is replaced once over the project life.

Four scheduled maintenance stops of 219 h, one per season, remove 876 h a year (90% availability). During a stop, the electrolyzer and the reactors are down, the battery can still be charged from the photovoltaic field, the rest of the generation is curtailed, and the whole CO_2 stream is sold.

The plant is simulated for a single year, but its cost is levelized over a project life of $n = 20$ years, during which the photovoltaic field, the electrolyzer and the battery degrade. Repeating the hourly simulation for each of the twenty years would multiply the computing time by twenty, which is not affordable inside the optimization. Instead, each degrading quantity is represented by one constant factor, chosen so that a single simulated year reproduces the discounted sums of the full project life. Because the levelized cost divides discounted costs by discounted energy, each year t of the project counts in proportion to its discount factor w_t. The equivalent factor of a quantity X is therefore the discount-weighted average of its year-by-year value $f_X(t)$:

$$\bar{f}_X = \frac{\sum_{t=1}^{n} w_t\ f_X(t)}{\sum_{t=1}^{n} w_t}, \qquad w_t = (1+r)^{-t} \tag{13}$$

where $f_X(t)$ is the fraction of its initial value that quantity X retains in year t and r is the discount rate. When the degradation is linear in time, this average equals the value of f_X in a single representative year, $t_{\mathrm{node}} = \Sigma\ t\ w_t / \Sigma\ w_t$, which for $r = 8\%$ and $n = 20$ is year 8.0 rather than the mid-life year 10.5, because discounting gives more weight to the early years. Three quantities are degraded where they act physically. The photovoltaic output is multiplied by 0.977 (linear degradation of 0.3% per year). The hydrogen produced per unit of electrolyzer power is multiplied by 0.970. This corresponds to a loss of 1.25×10^{-6} per operating hour, in line with the DOE target [40], reset when a stack is replaced at 60,000 h, within the range reported in [41]. The usable battery capacity is multiplied by 0.913. Capital costs are not reduced by degradation. This single-point approach was checked against a full year-by-year levelization for four plant configurations; the two agree within 0.25% of the levelized cost.

Catalyst deactivation is not modelled as a performance loss: the reactors run with fresh catalyst, and deactivation enters as the cost of three replacements of the 1085 kg charge over the project life (Section 3.5). One replacement every five years is a conservative assumption: a full-scale reactor with a commercial Ni/Al_2O_3 catalyst methanated

biogas for 1000 h without measurable deactivation [42], provided sulfur compounds are removed upstream.

3.5. Techno-Economic Framework

Three levelized costs are reported. The levelized cost of SNG (LCOSNG), the reference indicator of this work, and the levelized cost of methane (LCOM) share the same numerator. LCOSNG refers to the lower heating value of the whole product stream (47.63 MJ/kg), including its hydrogen and CO, and LCOM to that of the methane it contains (50.0 MJ/kg). LCOSNG is comparable with the price of natural gas and LCOM with studies that report on a pure-methane basis. The levelized cost of hydrogen (LCOH) covers only the hydrogen subsystem (photovoltaic field, battery, grid connection, electrolyzer, and hydrogen compression and storage) and places the hydrogen produced here against the electrolysis literature. All three follow

$$\mathrm{LCOX} = \frac{\mathrm{TCR} \cdot \mathrm{CRF} + \mathrm{OPEX_{net}}}{E_X}, \qquad \mathrm{CRF} = \frac{r\,(1+r)^n}{(1+r)^n - 1} \tag{14}$$

where TCR is the total capital requirement, CRF the capital recovery factor, $\mathrm{OPEX_{net}}$ the annual operating cost net of by-product credits and E_X the annual energy of the product (LHV). The project life n is 20 years, and the real discount rate r is 8%, the midpoint of the 6% and 10% scenarios used by IRENA for green hydrogen [41], which are also the sensitivity bounds.

Capital costs are built bottom-up (Table 4). Reactors are costed with the correlations of Turton et al. [43] as tubular units on their tube area, with pressure and material factors; heat exchangers and drums with a power law in area and pressure; and compressors with the power law of Woods [44], as tabulated by Andreasen et al. [45], evaluated at the maximum shaft power reached over the year. All are updated to a CEPCI of 806.9. The hydrogen compressor carries a service factor of 5 because delivering hydrogen at 214 bar requires an API 618 reciprocating unit with seals and materials resistant to embrittlement. The battery, electrolyzer and grid connection are costed from unit costs provided by EPC companies, and the PV field, hydrogen vessel and dehydration unit from recent literature (Table 4).

The purchased equipment cost is escalated to the total capital requirement as follows: piping 8%, electrical 4% and instrumentation 4% of the purchased equipment; materials 7% and labour 20% of the total purchase cost; engineering 7% of the bare erected cost; project and process contingencies of 20% each; and owner's costs of 7% of the total plant cost. The photovoltaic field and the battery are procured turnkey, so their unit costs already include erection, cabling, control and labour; they carry only engineering, a project contingency of 8% and owner's costs. The reactors and heat exchangers go through the full cascade, which provides an allowance for the steam circuit, control, start-up heating and catalyst handling of the methanation section. The grid connection (500 k€ per MW contracted) is added directly to the total capital requirement, and catalyst replacement is charged as an operating cost. The contracted power also limits the export of curtailed photovoltaic energy: only the part that fits through the connection is sold.

Stack replacements are charged as the stack life consumed beyond the first unit, prorated continuously. A stack costs 20% of the electrolyzer investment and lasts 60,000 operating hours; with 7238 operating hours per year, the base case consumes 2.41 stack lives in 20 years and is charged 1.41 replacements. Prorating avoids artificial steps in the sensitivity and optimization results. The battery is replaced once, at its full initial cost.

Operating costs are listed in Table 5. Items on the reactor side (methanation O&M, CO_2 purchase, catalyst replacement and TEG make-up) are charged to the plant only. Items on the photovoltaic, battery and electrolyzer side, including the credits for oxygen

and curtailed photovoltaic energy, are charged both to the plant and to the hydrogen subsystem. Personnel and insurance are shared in proportion to capital, and the RFNBO certification fee stays with the SNG. Since there is no CO_2 network at the site, the surplus CO_2 is resold at the purchase price less 20 €/t, to cover conditioning, transport and the margin of the buyer. Converting a tonne of CO_2 instead of reselling it saves this discount and about 4.8 €/t of compression electricity, some 5 €/MWh on the additional SNG. The discount varies between 0 and 40 €/t in the sensitivity analysis.

Table 4. Capital cost basis.

Item	Cost Basis	Source
PV field (turnkey)	671 USD/kW	[46]
Lithium-ion battery (turnkey)	166 USD/kWh	EPC data
PEM electrolyzer (incl. BoP)	850 USD/kW	EPC data
Compressed H_2 vessel	222 USD/kg	[47]
CO_2 compressors	1.35 MUSD $(P/1\ \mathrm{MW})^{0.9}$	[45]
H_2 compressor	×5 service factor on the H_2 train	—
Catalyst, initial charge	150 €/kg	Vendor
TEG dehydration	320 k€	[37]
Grid connection (PPA)	500 k€ per MW contracted	EPC data
Exchange rate; cost index base	0.866 €/USD; CEPCI 806.9	—

Table 5. Operating cost and by-product credit basis.

Item	Basis
PV O&M	5000 €/MW_{AC}·yr
PV land lease	1800 €/ha·yr at 1.7 ha/MW_{AC}
Grid electricity (PPA)	35 €/MWh
Grid network charges	12 €/MWh
Electrolyzer O&M	2% of electrolyzer investment per year
Water	2 €/m^3 (all-inclusive)
H_2 storage/compression/auxiliaries O&M	1.5/4.5/1% of investment per year
Methanation O&M	5% of investment per year
TEG make-up	1 k€/yr
CO_2 purchase	70 €/t of contracted stream
Catalyst replacement	3 replacements in 20 years at 150 €/kg
RFNBO certification	150 k€/yr
Personnel	8 persons × 40 k€/yr
Insurance	1% of TCR per year
Credit: oxygen sale	120 €/t
Credit: steam export	30 €/MWh
Credit: curtailed PV sold to grid	35 €/MWh, up to the grid connection rating
Credit: surplus CO_2 sale	50 €/t (purchase price less 20 €/t)

3.6. Optimization

The sizing of the plant is posed as a bound-constrained optimization of the hourly model. With x the vector of capacities and x_{lo}, x_{hi} its bounds, the single-objective problem is

$$\min_{\mathbf{x}} \mathrm{LCOSNG}(\mathbf{x}) \quad \text{subject to} \quad \mathbf{x}_{\mathrm{lo}} \le \mathbf{x} \le \mathbf{x}_{\mathrm{hi}} \tag{15}$$

where each evaluation is a complete simulation of the year followed by the cost model, so the objective is the levelized cost of Section 3.5 and not a surrogate. The rule-based

dispatch, with thresholds, a turndown floor and a hysteresis band, makes the objective non-smooth, so derivative-free population methods are used.

The decision variables are the six capacities marked in Table 2: photovoltaic field, battery energy and power, electrolyzer nominal power, contracted grid power and hydrogen buffer. The electrolyzer power can be varied because its correlation is used in the normalized form of Equation (10). The search ranges (Table 6) are wide so that the bounds do not decide the result. The CO_2 flow is not a decision variable since it fixes the scale of the plant. Neither are the reactor design, the operating temperatures and the feed ratio, which are embedded in the correlations of Table A1; changing them would take the model outside the range where those correlations are valid, and the code prevents it.

Table 6 lists the settings. The single-objective search uses differential evolution (DE/rand/1/bin) with ten individuals per decision variable, $F = 0.6$ and $CR = 0.9$. The multi-objective search uses NSGA-II with simulated binary crossover and polynomial mutation. Both methods are stochastic, so each configuration is run with five seeds and the spread between runs is reported as a measure of convergence.

A single-objective run stops after a fixed number of generations, or earlier if the best objective improves by less than 0.05% over twenty generations. Each optimum is then re-simulated, checked against the validity range of every correlation, and verified with a local sweep of ±20% on each variable.

Table 6. Settings of the sizing optimization. d is the number of decision variables and N the population size.

Item	Setting
Objective (single)	Minimize LCOSNG
Objectives (multi)	Minimize LCOSNG; maximize the share of the biogenic CO_2 converted, with the contracted grid power fixed at 5 MW (d = 5)
Decision variables, d	6
PV field	1–40 MW_{AC} (base 15)
Battery energy	0.5–40 MWh (base 10)
Battery power	0–20 MW (base 5), capped at 1 C
Electrolyzer nominal power	5–20 MW (base 10)
Contracted grid power	0–12 MW (base 5)
Hydrogen buffer	100–10,000 kg (base 3000)
DE: population, F, CR	$N = 10d = 60$; $F = 0.6$; $CR = 0.9$
DE: generations	80 per seed (4860 evaluations)
NSGA-II: population	$N = 100$
NSGA-II: operators	SBX $\eta_c = 15$, $p_c = 0.9$; polynomial $\eta_m = 20$, $p_m = 1/d$
NSGA-II: generations	120 per seed (12,100 evaluations)
Repetitions	5 seeds per configuration
Early stopping	<0.05% improvement of the best over 20 generations (single objective)
Local verification	±20% sweep of each variable around the optimum, 10 steps

Generative AI (Claude, Anthropic; Opus 5) was used to assist in writing and verifying the Python implementation of the hourly model, which was cross-checked against an independent spreadsheet implementation to machine precision, and in preparing the figures. All modelling decisions, input data and results were defined and checked by the authors.

4. Results and Discussion

4.1. On-Design Performance

The design point fixes the geometry of the plant: the CO_2 supply is at 850 kg/h, and the electrolyzer at its 10 MW nominal power. Table 7 gives the energy balance at this point and Table A2 the complete stream table for the streams of Figure A3.

The electrolyzer delivers 202.5 kg/h of hydrogen at 49.38 kWh/kg (67.5% efficiency, LHV). The reactors take 152.3 kg/h, and the remaining 50.2 kg/h are compressed into the buffer, so the design point already produces surplus hydrogen, and it sizes the hydrogen compression train. The electrolyzer splits 1811.6 kg/h of water. The reaction water condensed in the methanation section, 680.7 kg/h, could cover part of this demand after degassing and polishing, reducing the net make-up to 5.58 kg per kilogram of hydrogen.

The reactors convert 98.2% of the CO_2 and 99.3% of the hydrogen in a single pass. The product is 321.6 kg/h of SNG with 95.30 mol% CH_4 and a lower heating value of 47.63 MJ/kg (4254 kW). Figure 5 shows how the conversion is distributed along the two beds: most of it takes place in R1, and R2 acts as a polishing stage.

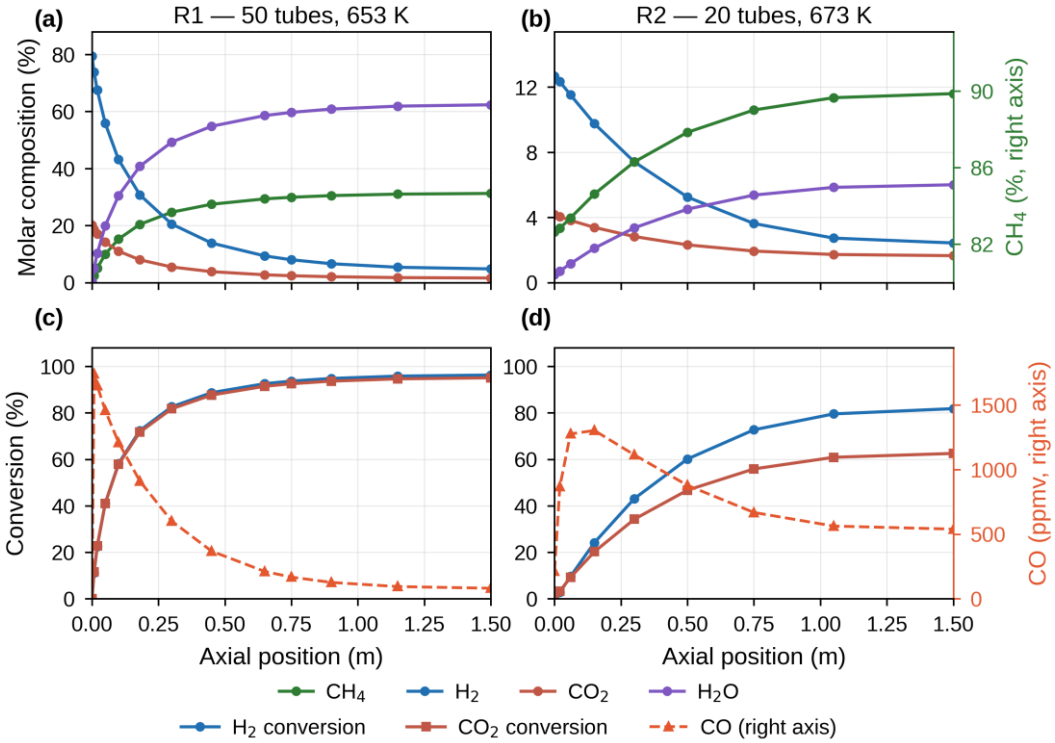

Figure 5. Axial profiles in the two methanation reactors at the design point. (**a**,**b**) Molar composition; (**c**,**d**) conversion and carbon monoxide content.

Compression is a minor consumer at this point: 127.4 kW, 1.3% of the plant demand. The export train is idle because the whole CO_2 stream is consumed.

Table 7. On-design energy balance of the plant.

Item	Value	Unit
Electric power demand		
PEM electrolyzer (EY1)	10,000	kW
H_2 compression to the buffer (K1, K2)	69.8	kW
CO_2 compression to the reactor (K3, K4)	57.5	kW
CO_2 compression for export (idle at this point)	0	kW
Water recirculation pump (P1)	0.01	kW

Total	**10,127.4**	**kW**
Thermal duties (negative: heat removed)		
E1, CO_2 intercooler	−27.8	kW
E2, H_2 intercooler	−41.8	kW
E3, H_2 aftercooler	−33.6	kW
E4, feed–effluent exchanger of R1 (recovered)	+213.6	kW
E5, feed–effluent exchanger of R2 (recovered)	+87.4	kW
E7, R1 effluent cooler	−434.6	kW
E8, R2 effluent cooler	−25.6	kW
V1, anode separator	−45.6	kW
R1, reaction heat	−893.6	kW
R2, reaction heat	−17.4	kW
Reaction heat raised as 15-bar saturated steam	**911.0**	**kW**
Steam raised (BFW at 105 °C)	1395.7	kg/h
Streams and performance		
H_2 produced	202.5	kg/h
to the reactor/to the buffer	152.3/50.2	kg/h
Specific electricity consumption of the electrolyzer	49.38	kWh/kg
Electrolyzer efficiency, LHV basis	67.5	%
O_2 by-product	1609.0	kg/h
Water split in the electrolyzer	1811.6	kg/h
of which recovered from methanation	680.7	kg/h
CO_2 fed to the reactor	850.0	kg/h
Single-pass conversion, CO_2/H_2	98.2/99.3	%
SNG produced	321.6	kg/h
CH_4 content, molar/mass basis	95.30/94.47	%
lower heating value	47.63	MJ/kg
thermal output	4254	kW
SNG output/H_2 input, LHV basis	83.8	%
Recovered reaction heat/H_2 input	17.9	%

4.2. Annual Operation

Table 8 summarizes the annual results. The photovoltaic field generates 33,226 MWh, of which 14.2% is curtailed, either because the electrolyzer is at its ceiling or because the plant is stopped for maintenance. Curtailed energy is all the photovoltaic energy that neither the electrolyzer nor the battery takes: 3040 MWh of it, about two thirds, is sold through the grid connection, and the remaining 1676 MWh arrives in hours when the export exceeds the 5 MW connection and is lost. The grid supplies 22,536 MWh: 21,927 MWh to the electrolyzer (43.6% of its electricity) and 609 MWh to the compressors. This contract keeps the reactor at a capacity factor of 76.0%, while the electrolyzer runs at 57.4%.

The plant converts 5658 t/y of CO_2 into 2140 t/y of SNG and sells the remaining 1788 t/y, so 24.0% of the contracted CO_2 leaves the plant unconverted. The annual specific consumption of the electrolyzer, 49.66 kWh/kg, is only 0.6% above its design value because the dispatch keeps the unit close to full load when it runs. The SNG contains 50.8% of the electricity available to the plant (photovoltaic generation plus grid import, LHV basis), or 61.7% if the exported heat is included; referred to the electricity actually consumed, which excludes the curtailed photovoltaic energy, the efficiency is 55.7%.The hydrogen fed to the reactor exceeds the hydrogen produced by 1.5 t because the buffer starts the year at half capacity and ends it empty; the effect on the cost is below 0.1%.

The hourly results also show how often the plant would go through the start-up and shut-down transients that the quasi-steady model omits. In the base case, the reactors run without interruption between maintenance stops: the electrolyzer stops for short periods,

2.3 h on average, but the hydrogen buffer keeps the reactors fed. In the optimal designs with a grid contract (Section 4.4), neither the electrolyzer nor the reactors stop outside maintenance. Only the photovoltaic-only design cycles the reactors, about once a day, so in that configuration, the heat-up and ramping periods would reduce the annual production below the value predicted here.

Table 8. Annual performance and cost summary of the base case.

Item	Value	Unit
Electricity		
PV generation	33,226	MWh
curtailed	4716 (14.2%)	MWh
sold to grid	3040	MWh
Grid (PPA) import	22,536	MWh
to the electrolyzer	21,927	MWh
Electricity to the electrolyzer	50,255	MWh
share from grid	43.6	%
Electricity to compression	609	MWh
Mass flows		
H_2 produced	1012.0	t
H_2 fed to the reactor	1013.5	t
H_2 routed through the buffer	117.4	t
CO_2 converted	5657.9	t
CO_2 sold unconverted	1788.1 (24.0%)	t
CH_4 produced	2022.2	t
SNG produced	2140.2	t
O_2 by-product	8031.9	t
Saturated steam at 15 bar	9291	t
Operation		
Electrolyzer capacity factor	57.4	%
operating hours	7238	h
Reactor capacity factor	76.0	%
hours at full load	3808	h
Hours with grid support active	4396	h
Scheduled maintenance	876	h
Battery equivalent full cycles	173.9	–
mean state of charge	33.6	%
H_2 buffer, mean/maximum inventory	95/538	kg
Performance		
Specific electricity consumption of the electrolyzer	49.66	kWh/kg
Electricity-to-SNG efficiency, LHV basis	50.8	%
including the exported heat	61.7	%
CH_4 content of the SNG, molar basis	95.30	%
Cost		
Purchased equipment cost	23.34	M€
Total capital requirement	44.56	M€
Operating cost, gross	2.958	M€/y
By-product credits	1.342	M€/y
Operating cost, net	1.617	M€/y
LCOSNG	**217.4 (2.876 €/kg)**	**€/MWh**
LCOM	**219.2 (3.044 €/kg)**	**€/MWh**
LCOH	**155.0 (5.166 €/kg)**	**€/MWh**

Figure 6 shows the hourly operation in a typical winter week and a typical summer week. The daily pattern is the same in both: the electrolyzer runs on grid power at night, rises with the sun, saturates the reactor and sends the surplus hydrogen to the buffer. In summer, the photovoltaic peak exceeds the ceiling of the electrolyzer, so the battery fills early and curtailment appears at midday; in winter, there is no curtailment. In both seasons, the buffer empties every night, as expected from a daily store.

Figure 7 aggregates the operation by month. The seasonal contrast is smaller than the solar resource suggests because the grid share of electricity rises from about 30% in summer to about 60% in winter. The four months with a maintenance stop produce less and sell more CO_2, and they account for 77% of the annual curtailment, which suggests that the maintenance calendar, fixed here, is also worth optimizing.

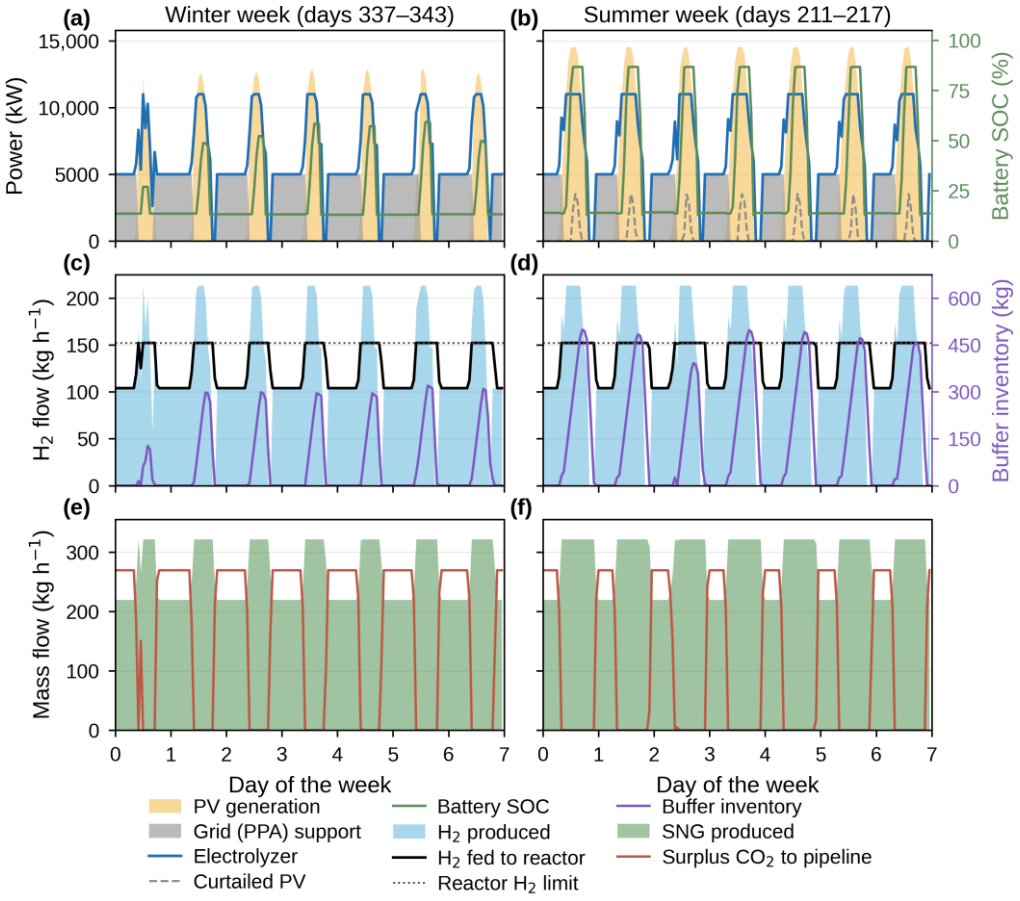

Figure 6. Hourly operation over two representative weeks, chosen as those with irradiation closest to the median of their season. (**a**,**b**) Electricity; (**c**,**d**) hydrogen; (**e**,**f**) product streams.

Figure 8 breaks down the levelized cost. Annualized capital contributes 160.3 €/MWh and operating costs 104.5 €/MWh, while by-product credits return 47.4 €/MWh (oxygen 34.0, steam 6.4, curtailed photovoltaic energy 3.8 and surplus CO_2 3.2 €/MWh). By subsystem, the largest contributions are the electrolyzer (52.4 €/MWh, after the oxygen credit), the grid supply (46.4 €/MWh) and the photovoltaic field (39.3 €/MWh). Plant-wide items (personnel, insurance and RFNBO certification) add 32.3 €/MWh. The methanation section contributes 6.2 €/MWh, under 3% of the total. The cost of the SNG is therefore driven by the production of hydrogen, not by its conversion to methane. This is also what sets the gap with other sources of methane: on an energy basis, the base case costs about three times the average production cost of biomethane in the European Union, 75–80 €/MWh [48], and six times the 2025 average price of natural gas in the Iberian market, 36.0 €/MWh [49].

Figure 9 shows the annual energy flows. Of the 55,761 MWh that enter the plant, 16,521 MWh are lost in the electrolyzer and 4716 MWh are curtailed; these are the main targets for improvement. The hydrogen buffer handles 12% of the hydrogen fed to the reactor and the battery 1920 MWh, so both stores shift a few hours of production rather than carry large energy flows. The methane contained in the CO_2 feed (1 mol%) crosses the plant unreacted and accounts for 1.03% of the SNG sold.

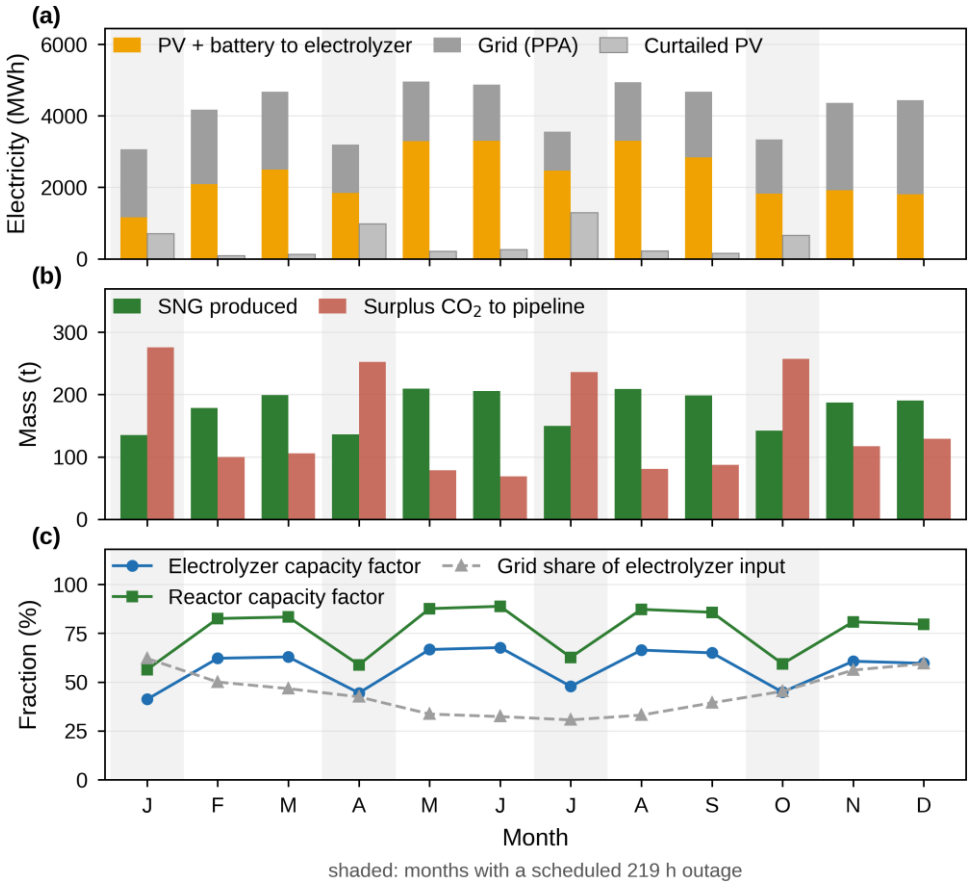

Figure 7. Monthly balance of the base case. (**a**) Electricity; (**b**) product and exported carbon dioxide; (**c**) capacity factors and share of grid electricity.

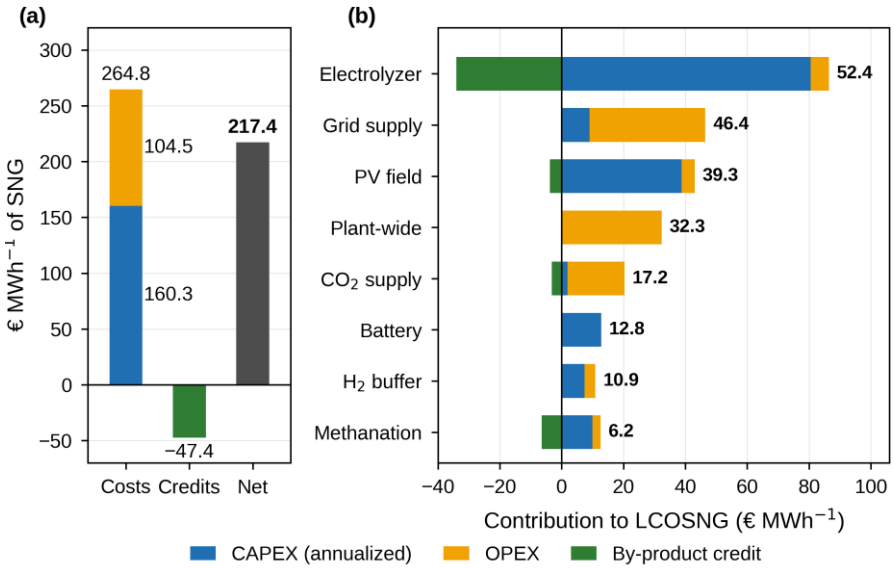

Figure 8. Breakdown of the levelized cost of synthetic natural gas. (**a**) Aggregate; (**b**) by subsystem, with each by-product credit assigned to the subsystem that generates it.

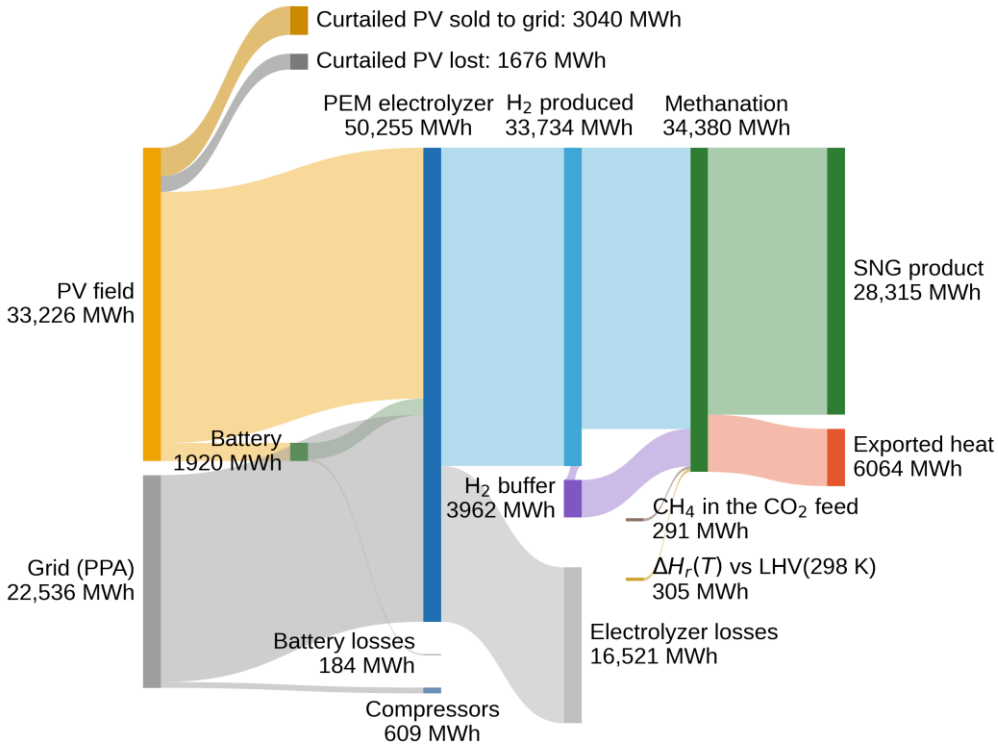

Figure 9. Annual energy flows of the base case (MWh, LHV basis).

4.3. Sensitivity Analysis

Each of the 27 parameters in Figure 10 was moved by ±25% from its base value, one at a time, and the whole year re-simulated. The CO_2 resale discount is the exception and was moved over its full range, 0 to 40 €/t. Structural parameters are excluded (Section 3.6). The degradation factors and the battery replacement count are recalculated whenever the discount rate, the project life or the degradation rates change.

Only seven parameters move the levelized cost by more than 10 €/MWh, and five of them are financial or capital parameters: the unit cost of the electrolyzer (±24.0 €/MWh), the indirect and contingency factors of Section 3.5 (−22.4/+25.5 €/MWh), the discount rate (−22.9/+24.3 €/MWh), the project life and the unit cost of the photovoltaic field. The other two, the electrolyzer power and the contracted grid power, are discussed below. The whole methanation section (reactors, catalyst, exchangers, drums and dehydration) stays within ±3.5 €/MWh and the compressors within ±1.0 €/MWh. The rigorous flowsheet is needed for credible balances, equipment sizes and off-design behaviour, but the cost of the product is decided upstream of the reactor.

Among the prices, the oxygen credit has the largest effect: a 25% lower oxygen price raises the cost by 8.5 €/MWh, and a 25% higher price lowers it by the same amount. In total, oxygen sales return 34.0 €/MWh; without any oxygen sale, the levelized cost would rise to 251.4 €/MWh, so the plant needs a neighbouring consumer that takes the oxygen under a long-term contract. The grid energy price follows (±7.0 €/MWh), then the CO_2 price (±3.5 €/MWh) and the network charges (±2.4 €/MWh). The CO_2 resale discount is worth ±1.3 €/MWh over its whole range and the heat export and the sale of curtailed photovoltaic energy less than 2 €/MWh each.

A discount rate of 6% or 10% gives 194.5 or 241.7 €/MWh. The project life and the PV field rating are the only parameter whose two bars point the same way: both 15 and 25 years are more expensive than 20. A shorter life raises the capital recovery factor. A longer one lowers it but adds a second battery replacement and more stack replacements, which outweigh the gain.

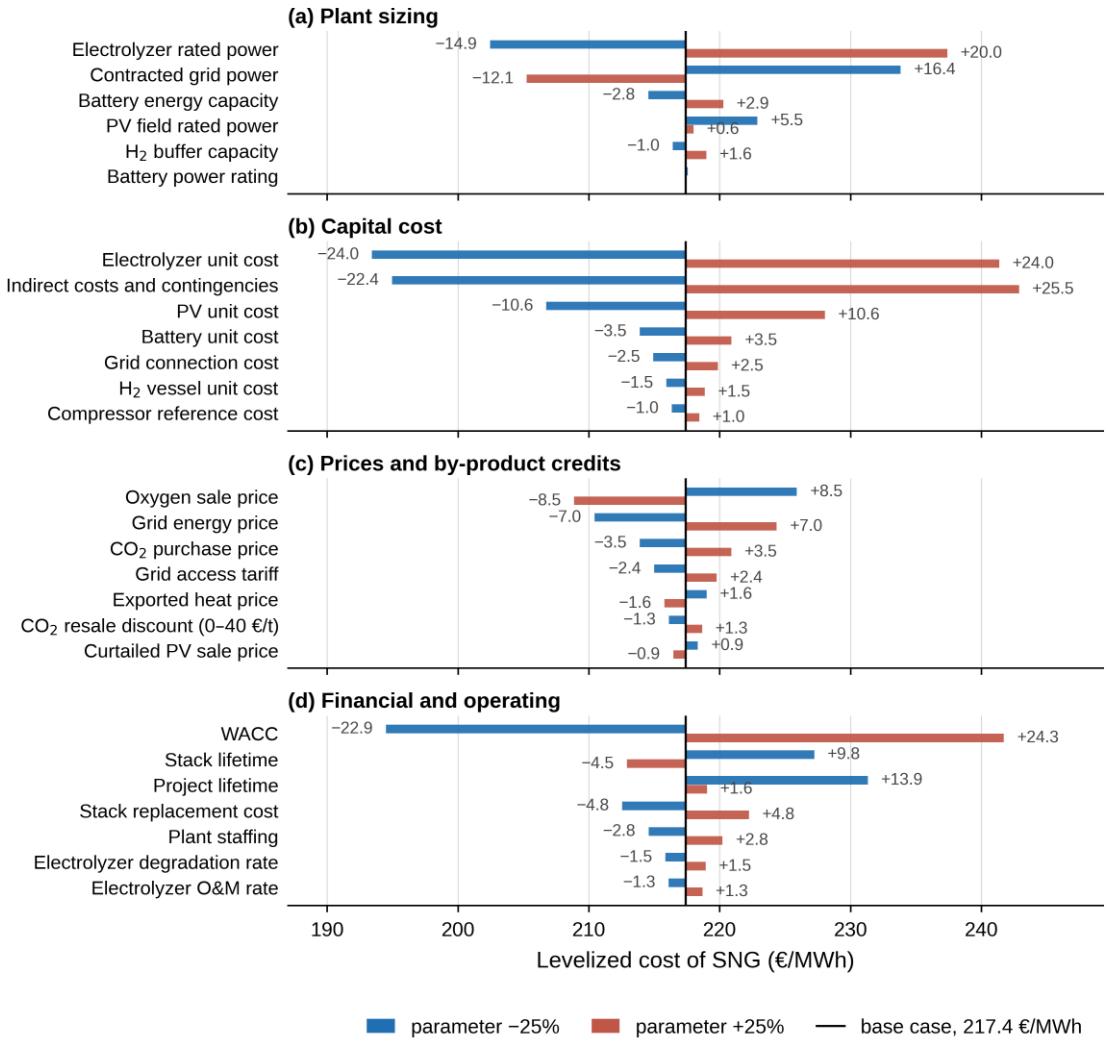

Figure 10. Sensitivity of the LCOSNG to a ±25% change in each parameter, one at a time (CO_2 resale discount: 0–40 €/t).

A one-at-a-time analysis does not capture interactions, and the most important one is between the two sources of electricity. Figure 11 maps the levelized cost over the photovoltaic power and the contracted grid power, with the electrolyzer at 10 MW and the rest of the plant at base values. The map is repeated for three grid energy prices, 35 €/MWh (base case), 55 and 75 €/MWh, with the network charges unchanged.

Below about 2 MW of contracted power, the cost rises sharply because the contract can no longer keep the electrolyzer above its 2 MW floor and the plant falls back to photovoltaic-only operation. Above that level, the maps have an interior optimum on both axes. The optimum contract is 7.5 MW at all three prices, close to the power the electrolyzer needs to saturate the reactors (Section 3.4). The optimum field is 14.8 MW at 35 €/MWh, practically the base case, and grows to 17.7 and 19.1 MW at 55 and 75 €/MWh. The minimum costs are 197.1, 215.7 and 233.4 €/MWh, up to 9.3% below the base design at the same price.

Photovoltaic energy is cheaper than grid energy: 42.8 €/MWh against 59.4 €/MWh in the base case, and 79.4 and 99.4 €/MWh at the higher prices. The optimum still asks for a larger contract because firm power increases the use of the equipment downstream: moving from the base case to the optimum at 35 €/MWh raises the electrolyzer capacity factor from 57.4 to 68.1% and the annual product by 18% for only 1.1 M€ more capital. The field size is then set by the cheaper photovoltaic energy. Figure 11d shows that at the three

optima, about half of the hydrogen is made from grid electricity, against 44.8% in the base case.

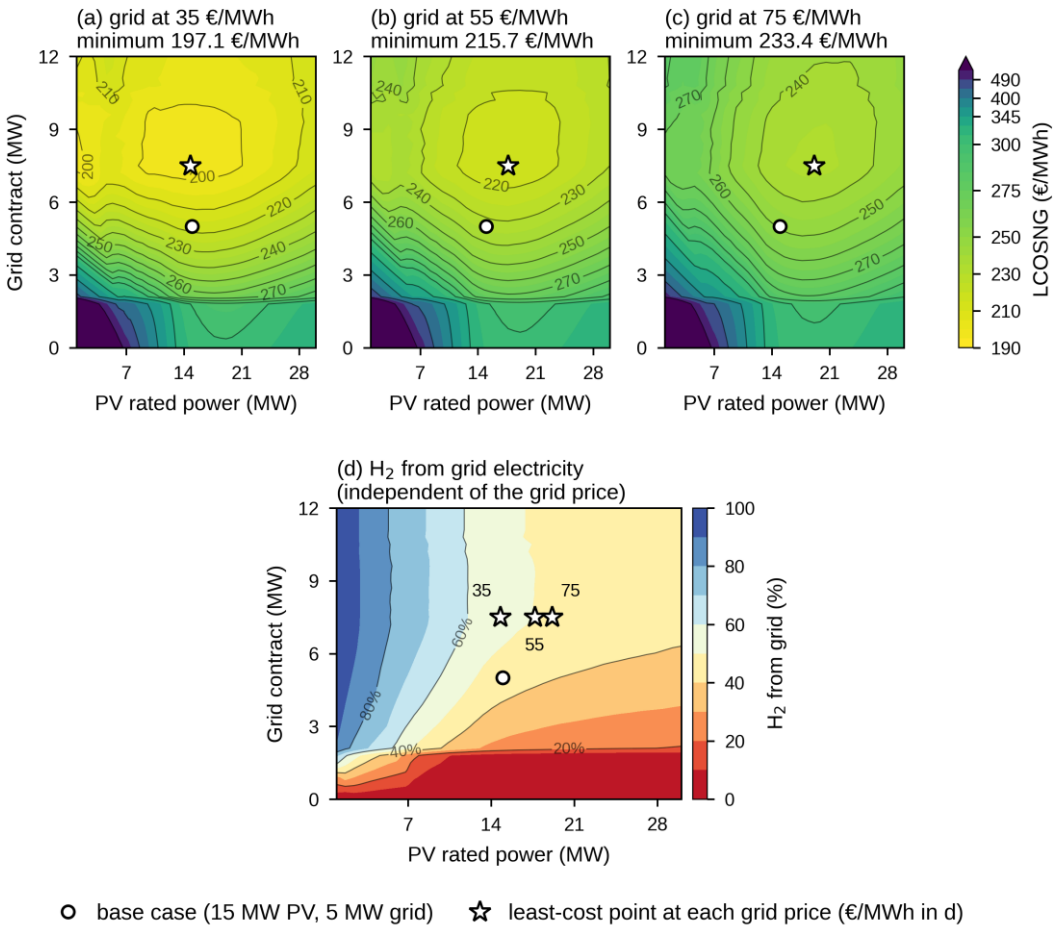

Figure 11. LCOSNG over the plane of photovoltaic power and contracted grid power, for a grid energy price of 35 €/MWh (**a**), 55 €/MWh (**b**) and 75 €/MWh (**c**). (**d**) Share of the hydrogen made from grid electricity, which does not depend on the price.

Figure 12 shows how the need for storage depends on the firm power available. Each panel sweeps the battery capacity (0.5–20 MWh, at 0.5 C) against the hydrogen buffer (200–5000 kg), with the electrolyzer at 10 MW, for a contracted power of 0, 2.5 and 5 MW. Without a grid contract, storage is what keeps the reactor running after sunset: a buffer of about 1160 kg lowers the cost by 29.4 €/MWh with respect to the smallest one, and a battery of about 3 MWh saves a further 3.2 €/MWh. As the contracted power increases, the grid takes over that role. The benefit of the buffer falls to 13.7 €/MWh with 2.5 MW and to 7.3 €/MWh with 5 MW, with its optimum at about 1000 kg in both cases, while the battery no longer brings any benefit: the cost rises steadily with its size, by about 23 €/MWh over the range, and the optimum stays at the smallest battery.

Hydrogen storage is therefore the cheaper option at every level of contracted power. Per unit of energy stored, the vessel costs about 7 USD per kWh of hydrogen (LHV), against 166 USD/kWh for the battery, and it stores the product that the reactor needs rather than the electricity that makes it. The battery only shifts photovoltaic energy that would otherwise be curtailed: it runs 174 equivalent full cycles a year in the base case, and removing it raises curtailment only from 14.2 to 20.1%. Reducing it from 10 to 0.5 MWh lowers the levelized cost of the base case by 11.0 €/MWh. The buffer, however, is only useful because the 10 MW electrolyzer produces more hydrogen than the reactors can take

at peak; when the electrolyzer is sized to the reactor, it becomes almost unnecessary (Section 4.4).

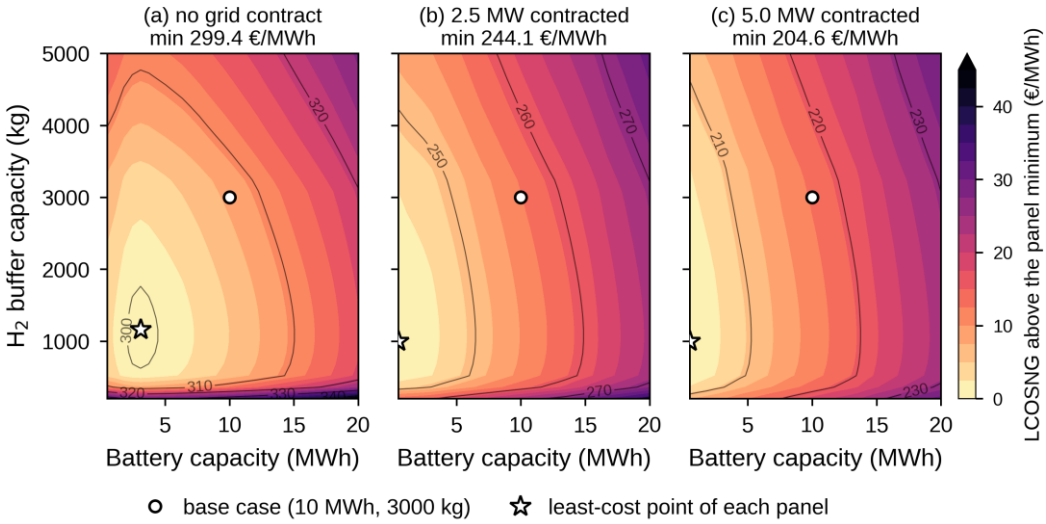

Figure 12. Levelized cost over the plane of battery capacity and hydrogen buffer capacity for a contracted grid power of 0, 2.5 and 5 MW. Filled contours give the excess over the minimum of each panel; labelled lines give the absolute value.

4.4. Sizing Optimization

The optimization of Section 3.6 was run in six configurations: all six capacities free; the contracted power fixed at 0, 2.5 and 5 MW; and the 5 MW case with a grid energy price of 55 and 75 €/MWh. The free configuration was also run at these two prices. Each configuration was solved with five seeds, which agreed within 0.12% of the best objective. Table 9 compares the optima with the base case.

Table 9. Optimal designs against the base case. Decision variables free in each configuration are in bold.

Item	Base Case	Free	0 MW	2.5 MW	5 MW	5 MW (55 €/MWh)	5 MW (75 €/MWh)
Decision variables							
PV field (MW_{AC})	15.00	**7.81**	**27.61**	**8.63**	**7.38**	**13.00**	**13.01**
Battery energy (MWh)	10.00	**0.50**	**2.99**	**0.50**	**0.50**	**0.50**	**0.50**
Battery power (MW)	5.00	**0.50**	**2.99**	**0.13**	**0.50**	**0.50**	**0.50**
Electrolyzer rated power (MW)	10.00	**7.13**	**17.09**	**5.32**	**5.67**	**6.91**	**6.91**
Contracted grid power (MW)	5.00	**7.85**	0.00	2.50	5.00	5.00	5.00
H_2 buffer (kg)	3000	**101**	**3493**	**100**	**152**	**100**	**100**
Annual performance							
SNG output (t/y)	2140	2535	1966	1249	1805	2000	2000
SNG output (MWh/y)	28,315	33,536	26,016	16,521	23,874	26,467	26,466
PV generation (MWh/y)	33,226	17,292	61,155	19,111	16,354	28,801	28,815
Grid import (MWh/y)	22,536	46,830	890	15,417	29,882	28,206	28,203
PV curtailment (%)	14.2	10.1	22.8	22.9	13.4	30.1	30.1
Electrolyzer capacity factor (%)	57.4	99.0	31.5	63.2	87.5	78.8	78.8
Reactor capacity factor (%)	76.0	90.0	69.8	44.3	64.1	71.0	71.0
CO_2 sold unconverted (%)	24.0	10.0	30.2	55.7	35.9	29.0	29.0
Grid share of electrolyzer electricity (%)	43.6	74.9	0.0	50.1	67.4	57.9	57.8
H2 produced from grid (%) *	44.8	74.9	0.0	51.5	67.9	58.7	58.7
Electricity-to-SNG efficiency, LHV (%)	50.8	52.3	41.9	47.8	51.6	46.4	46.4

Cost							
Purchased equipment (M€)	23.34	13.16	33.15	11.86	11.49	15.97	15.97
Total capital requirement (M€)	44.56	29.75	59.27	23.45	24.63	31.55	31.55
Operating cost, net (M€/y)	1.617	2.351	1.240	1.232	1.749	2.109	2.672
LCOSNG (€/MWh)	217.4	160.4	279.7	219.2	178.4	201.1	222.4
LCOSNG (€/kg)	2.876	2.123	3.701	2.900	2.360	2.660	2.942
LCOM (€/MWh)	219.2	161.8	282.1	220.9	179.8	202.7	224.2
LCOH (€/kg)	5.166	3.687	6.833	4.591	3.897	4.623	5.206

* Hydrogen is attributed hourly; the grid share of hydrogen exceeds that of electricity because grid-only hours run at part load, where the specific consumption is lower.

The unconstrained optimum costs 160.4 €/MWh, 26% below the base case. It combines a 7.1 MW electrolyzer, a 7.9 MW grid contract and a 7.8 MW photovoltaic field. The electrolyzer runs at a capacity factor of 99% and keeps the reactor at 90% of its capacity, the maximum allowed by the maintenance stops. The electrolyzer and the contract are both sized to the reactor: at its 110% ceiling, a 7.1 MW electrolyzer produces the 152 kg/h the reactors can take. The photovoltaic field is half that of the base case and supplies a quarter of the hydrogen. The battery and the buffer go to their lower bounds. This is not an effect of the bounds; Figure 12 shows the cost rising with battery size whenever there is a contract, and the buffer loses its purpose once the electrolyzer no longer produces more hydrogen than the reactors can take. Compared with the best point of Figure 11 (197.1 €/MWh), sizing the electrolyzer to the reactor and removing the battery save a further 37 €/MWh.

Without a PPA contract, the optimizer does the opposite: a 27.6 MW field, a 17.1 MW electrolyzer, a 3.0 MWh battery and a 3493 kg buffer, at 279.7 €/MWh. This is the only case in which the storage devices grow; with any contract, the battery falls to its lower bound and the buffer to 100–152 kg. The cost is 219.2 €/MWh with 2.5 MW and 178.4 €/MWh with 5 MW, so the first 5 MW of firm supply lower the cost by 101 €/MWh and the remaining 2.85 MW up to the free optimum by only 18 €/MWh more. At the base grid price, the field stays between 7.4 and 8.6 MW in all designs with a contract, and the electrolyzer between 5.3 and 7.1 MW.

With the 5 MW contract, raising the grid energy price to 55 and 75 €/MWh moves the optimum towards photovoltaic energy: the field grows from 7.4 to 13.0 MW, the electrolyzer from 5.7 to 6.9 MW, and the grid share of the hydrogen falls from 67.9 to 58.7%. The same design is optimal at both prices, and the cost rises to 201.1 and 222.4 €/MWh, about 1.1 €/MWh per €/MWh of grid energy. The optimum remains 27–39 €/MWh below the base design at each price. In the free configuration, the electrolyzer and contract stay at 7.1 and 7.9 MW, the field grows to 13.2 and 15.8 MW, and the cost rises to 186.9 and 211.3 €/MWh. A more expensive grid therefore does not change the structure of the least-cost plant, a reactor kept close to saturation with firm power, but it shifts part of the hydrogen production to the photovoltaic field. The least-cost plant therefore depends on firm grid supply: the free optimum makes three quarters of its hydrogen from grid electricity, against 45% in the base case and none in the photovoltaic-only design. This dependence exposes the cost to the grid price, but even at 75 €/MWh, the grid-supported optimum remains about 25% cheaper than the photovoltaic-only design. It also improves operational resilience since the reactors run continuously, whereas the photovoltaic-only design cycles them almost daily (Section 4.2) and leaves 30% of the CO_2 unconverted. Only the photovoltaic-only design qualifies as a renewable fuel of non-biological origin by construction, provided the field is new. The grid-supported designs would require renewable power purchase agreements, meeting the additionality and temporal correlation conditions of Delegated Regulation (EU) 2023/1184. Since 70–80% of their grid electricity is

drawn in hours without solar generation, hourly matching would call for wind rather than solar contracts, likely at a price premium covered by the 55 and 75 €/MWh cases.

The levelized cost is almost insensitive to how much of the available CO_2 is converted because converting a tonne instead of reselling it saves only about 5 €/MWh on the additional product (Section 3.5). The optimizer therefore converts only 44.3% of the stream with 2.5 MW and 64.1% with 5 MW, against 76.0% in the base case and 90.0% in the free optimum. The plant-wide fixed costs (personnel, insurance and RFNBO fee) are largely independent of the production, so per unit of product, they range from 22.9 €/MWh in the free optimum to 42.6 €/MWh in the 2.5 MW case.

Figure 13a shows how the cost moves between subsystems. From the base case to the free optimum, the photovoltaic field falls from 39.3 to 17.1 €/MWh and the grid supply rises from 46.4 to 77.6 €/MWh, so together they change little. The saving comes from the electrolyzer (52.4 to 19.9 €/MWh), which produces 18% more with 29% less rated power, from the battery (12.8 to 0.5 €/MWh) and from the plant-wide costs (32.3 to 22.9 €/MWh), spread over a larger production. Figure 13b confirms the optimum. The cost is almost flat in the battery, buffer and photovoltaic directions (under 1% over ±20%), whereas a 20% change in the electrolyzer power costs 7–11% and in the contracted power 2–5%. The two electrical capacities must be sized carefully; the others have a wide tolerance.

The single-objective optimum leaves open how much of the biogenic CO_2 the plant uses. With a free contract, this is not an issue: a multi-objective search collapsed onto a single point, at about 161 €/MWh and 90% conversion, because the least-cost design already converts all the CO_2 the maintenance calendar allows. The two objectives conflict only when firm power is limited. The multi-objective search of Table 6 therefore fixes the contract at 5 MW and treats the levelized cost and the share of CO_2 converted as competing objectives. Figure 14 shows the resulting front, 272 non-dominated designs from the five NSGA-II runs and the 5 MW single-objective optimum.

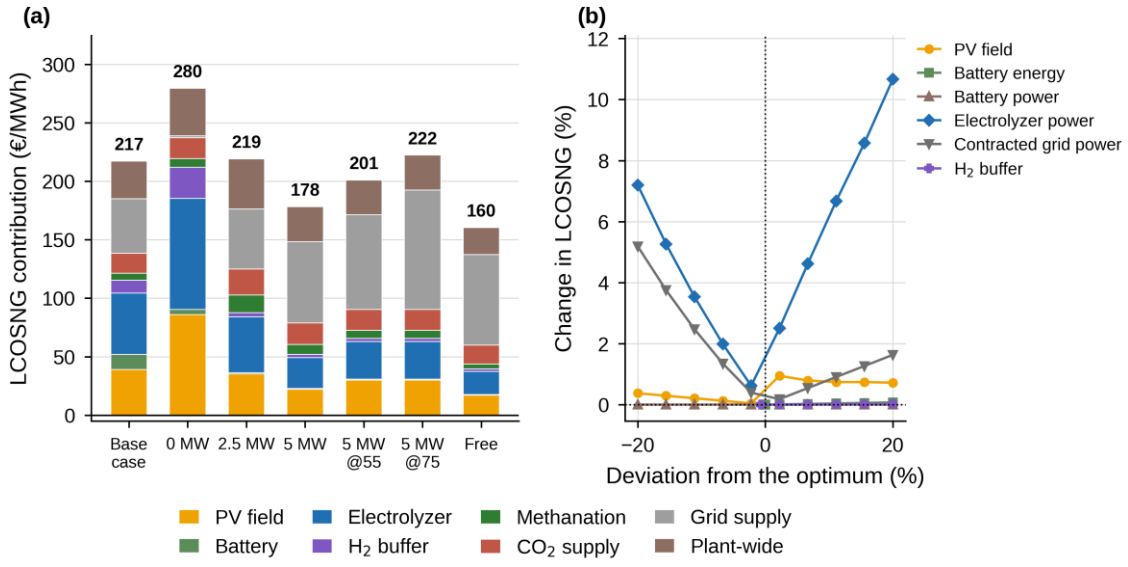

Figure 13. Optimal designs. (**a**) LCOSNG of the base case and of the optimal designs of Table 9 by subsystem. (**b**) Local verification of the unconstrained optimum, ±20% on each capacity.

The front goes from 178.4 €/MWh at 64.1% conversion to 337.7 €/MWh at 88.9%, in three stretches. Up to about 71%, it is almost flat (+1.6 €/MWh); the optimizer only enlarges the electrolyzer up to the size that the contracted power can supply, and the photovoltaic field keeps the reactor nearly full. Between 71% and 84%, each additional point costs about 5 €/MWh because the extra hydrogen must come from photovoltaic energy: the field grows to 27 MW, the electrolyzer to 16 MW and a buffer of about two tonnes reappears.

Above 86%, the cost rises steeply and the field and electrolyzer reach the bounds of the search, so this last stretch underestimates the cost of full conversion.

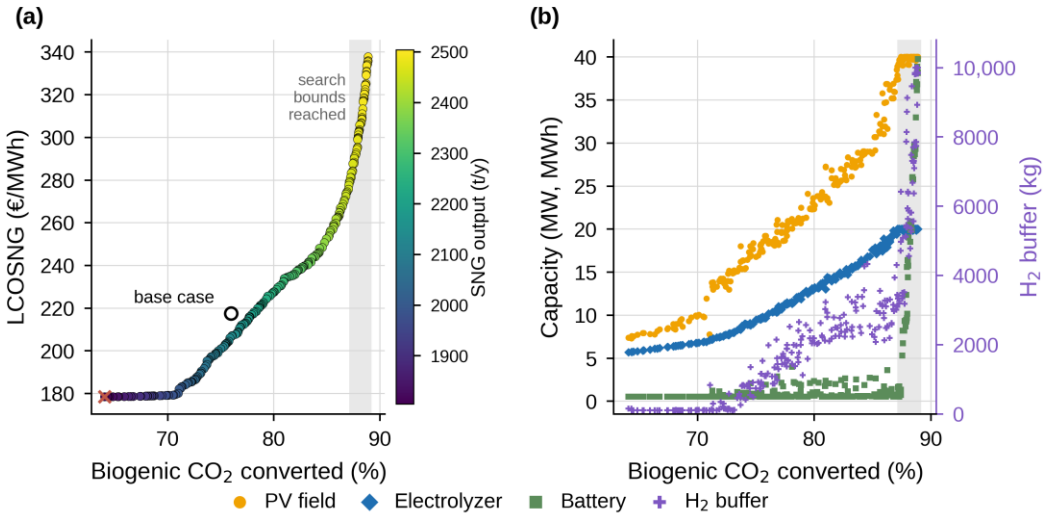

Figure 14. Pareto front between LCOSNG and the share of biogenic CO_2 converted, with the contracted grid power fixed at 5 MW. (**a**) Objective space, coloured by annual product; open circle: base case; cross: 5 MW single-objective optimum. (**b**) Decision variables along the front. In the shaded band the photovoltaic field and the electrolyzer reach their upper bounds.

The base case lies above the front: at its 76% conversion the front gives 206.7 €/MWh, 10.7 €/MWh less, with an 18.7 MW field, a 10.1 MW electrolyzer, a 1165 kg buffer and no battery. Because the contract is fixed, every additional point of conversion uses photovoltaic hydrogen, and the share of hydrogen made from grid electricity falls along the front from 68% to 3%. With a fixed contract, converting more biogenic CO_2 and producing a more renewable fuel are therefore the same decision, at about 5 €/MWh per percentage point between 71% and 84%.

5. Conclusions

This work assessed, hour by hour over a full year, a 10 MWe PEM electrolysis and catalytic methanation plant that converts the biogenic CO_2 of a biomethane upgrading unit in the Huelva chemical cluster. The model combines a rigorous AVEVA Process Simulation flowsheet, reduced to off-design correlations, with an hourly dispatch and cost model. The base case (15 MW photovoltaics, 10 MWh battery, 10 MW electrolyzer, 3000 kg hydrogen buffer and 5 MW grid contract) produces 2140 t/y of SNG with 95.3 mol% CH_4 at 217.4 €/MWh (2.88 €/kg), with a total capital requirement of 44.6 M€. The grid supplies 43.6% of the electricity used by the electrolyzer, and 24.0% of the CO_2 is sold unconverted. This cost lies within the 2.4–3.9 €/kg reported for comparable plants [20,22].

Sizing has a larger effect than any single price. The least-cost design has a 7.1 MW electrolyzer, sized to produce at full load the hydrogen the reactors can take, fed by a 7.9 MW grid contract and a 7.8 MW photovoltaic field, without a battery and with a minimal buffer. It reaches 160.4 €/MWh (2.12 €/kg), 26% below the base case. Photovoltaic energy is cheaper than grid energy (42.8 against 59.4 €/MWh), but firm grid power is what keeps the electrolyzer and the reactors fully used, and the battery does not pay for itself whenever a grid contract is available. The optimum costs 279.7 €/MWh without a contract and 178.4 €/MWh with 5 MW. The maintenance calendar, fixed here, concentrates most of the curtailment and could be optimized.

With the surplus CO_2 resold at 20 €/t below its purchase price, the cost-optimal plant has little incentive to convert more CO_2. With the contract fixed at 5 MW, raising the

conversion from 64% to 71% is almost free, each further point up to 84% costs about 5 €/MWh, and the cost rises steeply above 86%. The base case lies 10.7 €/MWh above this front. Along the front, the share of hydrogen made from grid electricity falls from 68% to 3%, so converting more biogenic CO_2 also makes the fuel more renewable.

These findings follow from the simulations, but some of them depend on assumptions external to the process: the availability and price of firm grid electricity, the sale of oxygen to a neighbouring consumer, and the conditions under which the SNG would qualify as a renewable fuel of non-biological origin. The grid-supported designs would require renewable power purchase agreements that comply with Delegated Regulation (EU) 2023/1184. The effect of these assumptions on the cost is discussed in Sections 4.3 and 4.4.

The main limitations of the model are its quasi-steady hourly resolution, which omits start-up and ramping transients that are relevant only in the photovoltaic-only design, and the isothermal representation of the reactors. Future work should validate the hourly operation against dynamic simulation or plant data and address the detailed thermal design of the methanation reactors.

Author Contributions: Conceptualization, C.O. and S.G.-L.; methodology, C.O. and C.M.-M.; software, C.O. and C.M.-M.; validation, C.M.-M. and S.G.-L.; formal analysis, C.O. and C.M.-M.; investigation, C.M.-M.; resources, C.O. and M.A.D.-P.; data curation, C.M.-M.; writing—original draft preparation, C.O.; writing—review and editing, C.M.-M., S.G.-L. and M.A.D.-P.; visualization, C.M.-M.; supervision, C.O. and M.A.D.-P.; project administration, C.O.; funding acquisition, C.O. All authors have read and agreed to the published version of the manuscript.

Funding: This research was funded by the European Union's Horizon Europe research and innovation programme under grant agreement No. 101235215 (METHCESFUEL: Renewable methanol-based synthetic multifuel production).

Data Availability Statement: The data supporting the findings of this study are available from the corresponding author upon reasonable request.

Acknowledgments: During the preparation of this manuscript, the authors used Generative AI (Claude, Anthropic (San Francisco, CA, USA); Opus 5) for the purposes of writing and verifying the Python implementation of the hourly model and in preparing the figures. The authors have reviewed and edited the output and take full responsibility for the content of this publication.

Conflicts of Interest: S.G.-L. is employed by Repsol Technology Lab. The remaining authors declare no conflicts of interest. Repsol had no role in the design of the study, the analyses or the decision to publish.

Abbreviations

The following abbreviations are used in this manuscript:

AC	Alternating current
API	American Petroleum Institute
BFW	Boiler feed water
BoP	Balance of plant
CEPCI	Chemical Engineering Plant Cost Index
CRF	Capital recovery factor
DC	Direct current
DE	Differential evolution
DOE	U.S. Department of Energy
EPC	Engineering, procurement and construction
IAPWS	International Association for the Properties of Water and Steam
IRENA	International Renewable Energy Agency

LCOH	Levelized cost of hydrogen
LCOM	Levelized cost of methane
LCOSNG	Levelized cost of synthetic natural gas
LHHW	Langmuir–Hinshelwood–Hougen–Watson
LHV	Lower heating value
NREL	National Renewable Energy Laboratory
NSGA-II	Non-dominated sorting genetic algorithm II
NSRDB	National Solar Radiation Database
O&M	Operation and maintenance
OPEX	Operating expenditure
PEM	Proton exchange membrane
PFR	Plug-flow reactor
PPA	Power purchase agreement
PSRK	Predictive Soave–Redlich–Kwong
PV	Photovoltaic
RFNBO	Renewable fuel of non-biological origin
SBX	Simulated binary crossover
SNG	Synthetic natural gas
TCR	Total capital requirement
TEG	Triethylene glycol
TMY	Typical meteorological year

Appendix A

Appendix A.1. Electrolyzer Polarization Curve

The electrochemical submodels of Section 3.2 (Equations (1)–(7)) were compared with the polarization curve measured by Espinosa-López et al. on a 46 kW high-pressure PEM electrolyzer at 50 °C and an anode pressure of 35 bar [31]. The 41 experimental points were digitized from Figure 6b of that work, between 0.006 and 1.43 A/cm^2. Figure A1 compares them with the model published by the same authors, with their fitted parameters, and with the model of this work for two values of the membrane water content: $\lambda = 22.2$, which gives practically the same protonic conductivity as the membrane fitted by Espinosa-López et al., and $\lambda = 14$, the value adopted in this work. The flowsheet model was solved at the conditions of the test at several current densities (squares in Figure A1), and the same equations were then evaluated at every experimental point; both sets of values agree within 0.01 mV.

With $\lambda = 22.2$, the model reproduces the experimental curve with a root mean square error of 5 mV and a maximum deviation of 11 mV, practically the same accuracy as the model of Espinosa-López et al. (4 and 10 mV). With $\lambda = 14$, the activation region is still well reproduced, but the cell voltage is overestimated by an amount that grows with current density, up to 114 mV (6.3%) at 1.43 A/cm^2, because the lower conductivity raises the ohmic slope from about 0.15 to 0.23 V per A/cm^2.

$\lambda = 14$ is therefore a conservative choice. At the design conditions of this work (80 °C, 21.5 bar, 1.49 A/cm^2), it gives a cell voltage of 1.851 V and a stack consumption of 49.4 kWh/kg, against 1.769 V with $\lambda = 22.2$. The adopted value keeps the electricity demand of the electrolyzer in line with commercial PEM stacks [40] and provides a margin for membrane ageing and for the losses not represented in the model.

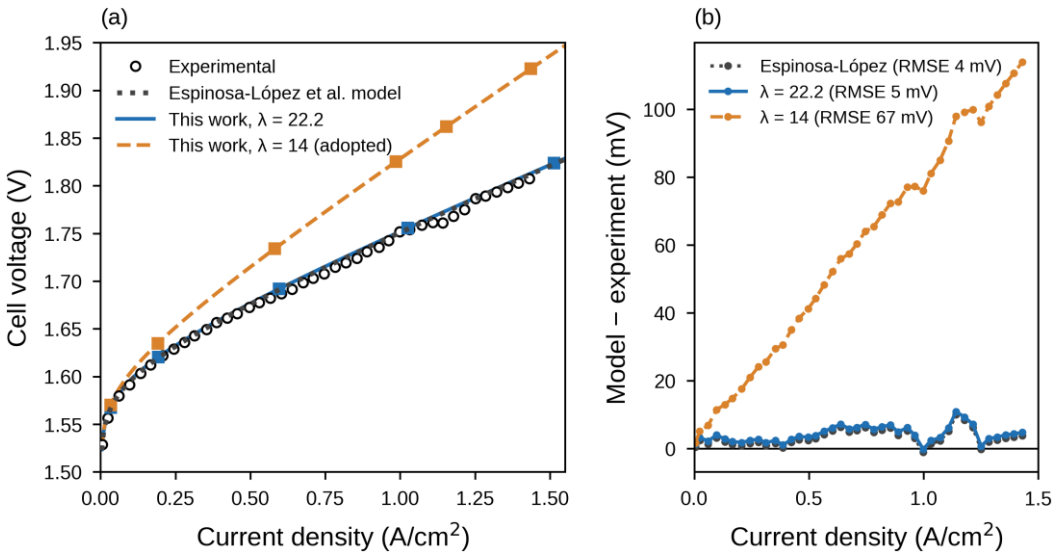

Figure A1. Polarization curve of a 46 kW PEM electrolyzer at 50 °C and 35 bar [31] compared with the model of Espinosa-López et al. and with the model of this work for $\lambda = 22.2$ and $\lambda = 14$ (adopted). (**a**) Cell voltage against current density; squares are solutions of the flowsheet model. (**b**) Deviation of each model from the experimental values.

Appendix A.2. Validation of the Kinetic Implementation

The kinetic submodel was checked at two levels (Figure A2). First, its implementation in AVEVA Process Simulation was verified against an independent integration of the same rate equations, written in Python with an implicit solver for stiff systems, for an isothermal plug-flow reactor without pressure drop. Twenty conditions were compared: five temperatures between 573 and 673 K at 10 bar with a stoichiometric feed ($H_2/CO_2 = 4$) in the differential regime, and fifteen conditions at 10 bar with $H_2/CO_2 = 1$, covering the space times of the methanation experiments of Xu and Froment. The two solutions agree within 0.33% in conversion (Figure A2c), and in the differential tests, the CH_4 and CO fractions coincide to the fourth decimal place, which confirms that the three reactions of the scheme, and not only the overall CO_2 consumption, are correctly resolved.

Second, the model was compared with the experiments from which Xu and Froment derived the kinetics [15]. For methanation, the data of their Figure 5 (10 bar, $H_2/CO_2 = 1$, 573–673 K) were digitized. With the original parameter set, the model reproduces the effect of temperature and space time but underestimates the conversion of CO_2 into methane by 9.6% on average, with a root mean square deviation of 0.007 in conversion (Figure A2a). The largest relative deviations occur at 573 K, where conversions are below 2% and the uncertainty of the digitized points is largest. Applying the activity factor of 1.225 used in later studies would reverse this bias (mean deviation +5.6%). The original parameters were kept since a lower conversion is on the conservative side for the design of the reactors.

For steam reforming, the model was compared with the data of their Figure 3 at 773 and 848 K (10 bar, $H_2O/CH_4 = 3$). The mean deviation in the conversion of methane into CO_2 is +0.3% at 773 K and −5.3% at 848 K, with maximum deviations of 6.8% and 9.5% (Figure A2b). The kinetic model therefore reproduces the experimental data in both directions of the reactions within about 10%.

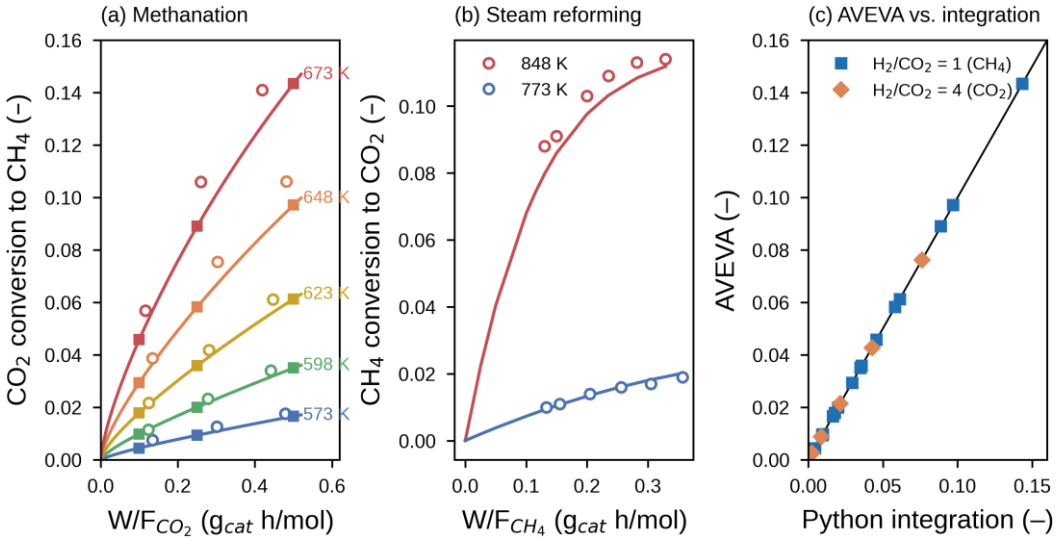

Figure A2. Validation of the kinetic submodel against the experiments of Xu and Froment [15]. (**a**) Conversion of CO_2 into CH_4 at 10 bar and $H_2/CO_2 = 1$; circles: experimental data, digitized from their Figure 5; lines: model; squares: flowsheet (AVEVA) solutions. (**b**) Conversion of CH_4 into CO_2 in steam reforming at 10 bar and $H_2O/CH_4 = 3$; circles: experimental data; lines: model. (**c**) Conversion calculated by AVEVA against the independent integration of the rate equations.

Appendix A.3. Off-Design Performance Correlations

Table A1. Performance correlations fitted to the off-design flowsheet and used in the hourly model. P: electrolyzer power (kW). m: hydrogen fed to methanation (kg/h); F: CO_2 stream flow through the train (kg/h); p_{tank}: buffer pressure (kPa).

Correlation	Form	Coefficients	Range; R^2
H_2 production, kg/h	$a \cdot P^2 + b \cdot P + c$ (P in kW)	$a = -2.3578 \times 10^{-7}$; $b = 2.2591 \times 10^{-2}$; $c = 0.2293$	2–11 MW; 0.99999
CO_2 to methanation, kg/h	$a \cdot m$	$a = 5.58244$	10–152.3 kg/h; 1.000000
CH_4 produced, kg/h	$a \cdot m + b \cdot m^2$	$a = 1.99599$; $b = -5.7962 \times 10^{-6}$	10–152.3 kg/h; 0.99999998
SNG produced, kg/h	$a \cdot m + b \cdot m^2$	$a = 2.10992$; $b = 1.2982 \times 10^{-5}$	10–152.3 kg/h; 0.99999992
Reaction heat R1 + R2, kW	$a \cdot m + b \cdot m^2$	$a = 5.98631$; $b = -2.1225 \times 10^{-5}$	10–152.3 kg/h; 0.99999997
Steam at 15 bar, kg/h	$a \cdot m + b \cdot m^2$	$a = 9.17138$; $b = -3.2518 \times 10^{-5}$	Derived from heat
CO_2 compression to methanation, kW	$a \cdot F + b \cdot F^2$	$a = 6.7701 \times 10^{-2}$; $b = 1.907 \times 10^{-6}$	0–850 kg/h; 0.999998
CO_2 compression for export, kW	$a \cdot F + b \cdot F^2$	$a = 0.100705$; $b = 4.097 \times 10^{-6}$	0–850 kg/h; 0.999997
H_2 compression to buffer, kW	$A \cdot \dot{m} \cdot [(p_{tank}/p_1)^n - 1]$ ($\dot{m}$ in kg/s)	$A = 33{,}496$; $p_1 = 2085$ kPa; $n = 0.05991$	0–50.2 kg/h; 0.9988

Appendix A.4. On-Design Flowsheet and Stream Table

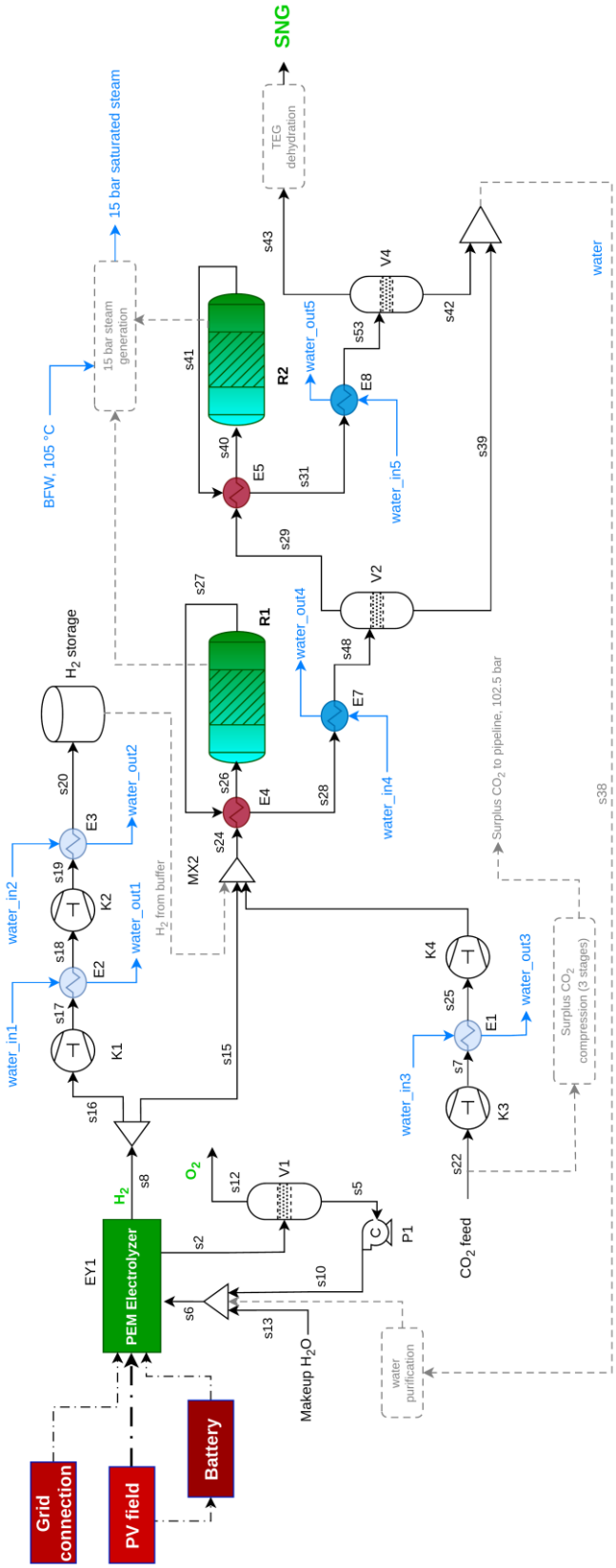

Figure A3. Detailed process flow diagram of the plant at the design point, with the equipment and stream labels used in the text and in Table A2.

Table A2. Stream table of the design-point flowsheet (CO_2 feed 850 kg/h, electrolyzer at 10 MW). Stream labels are those of Figure A3. *VF*: molar vapour fraction. Compositions are molar percentages; nitrogen is below 10^{-6} mol% in every stream and is omitted.

Stream	Description	$\dot{m}$ (kg/h)	T (°C)	p (bar)	VF	H_2	H_2O	CH_4	CO_2	CO	O_2
s13	Demineralized water make-up	1811.55	30.0	22.00	0.000	–	100.000	–	–	–	–
s10	Recycled water from V1	199.27	30.0	21.50	0.000	–	99.958	–	–	–	0.042
s6	Water fed to EY1	2010.82	30.0	21.50	0.000	–	99.996	–	–	–	–
s2	Anode outlet (O_2 + water)	1808.31	79.7	21.00	0.838	–	18.181	–	–	–	81.819
s12	Oxygen by-product	1609.04	29.9	20.50	1.000	–	0.216	–	–	–	99.784
s5	Water drained from V1	199.27	30.0	21.00	0.000	–	99.958	–	–	–	0.042
s8	Hydrogen from EY1	202.51	80.0	20.90	1.000	100.000	–	–	–	–	–
s15	H_2 routed to the reactor	152.26	80.0	20.90	1.000	100.000	–	–	–	–	–
s16	H_2 routed to the buffer	50.24	80.0	20.90	1.000	100.000	–	–	–	–	–
s17	K1 discharge	50.24	253.7	66.88	1.000	100.000	–	–	–	–	–
s18	E2 outlet	50.24	47.9	66.83	1.000	100.000	–	–	–	–	–
s19	K2 discharge	50.24	207.5	213.86	1.000	100.000	–	–	–	–	–
s20	To H_2 buffer	50.24	43.3	213.81	1.000	100.000	–	–	–	–	–
s22	CO_2 feed	850.00	30.0	1.20	1.000	–	1.500	1.000	97.500	–	–
s7	K3 discharge	850.00	162.0	5.04	1.000	–	1.500	1.000	97.500	–	–
s25	E1 outlet	850.00	38.7	4.99	1.000	–	1.500	1.000	97.500	–	–
s24	Reactor feed (H_2 + CO_2)	1002.26	102.4	20.90	1.000	79.387	0.309	0.206	20.098	–	–
s26	E4 outlet, R1 inlet	1002.26	352.2	20.85	1.000	79.387	0.309	0.206	20.098	–	–
s27	R1 outlet	1002.26	380.0	20.84	1.000	4.790	62.350	31.254	1.598	0.008	–
s28	E4 shell outlet	1002.26	184.9	20.79	0.866	4.790	62.350	31.254	1.598	0.008	–
s48	E7 outlet	1002.26	41.0	20.74	0.378	4.790	62.350	31.254	1.598	0.008	–
s29	V2 vapour	343.23	41.0	20.74	1.000	12.666	0.496	82.638	4.178	0.021	–
s39	V2 condensate	659.04	41.0	20.74	0.000	0.004	99.934	0.032	0.030	–	–
s40	E5 outlet, R2 inlet	343.23	364.1	20.69	1.000	12.666	0.496	82.638	4.178	0.021	–
s41	R2 outlet	343.23	400.0	20.69	1.000	2.429	6.002	89.864	1.650	0.054	–
s31	E5 shell outlet	343.23	95.3	20.64	0.988	2.429	6.002	89.864	1.650	0.054	–
s53	E8 outlet	343.23	32.0	20.59	0.943	2.429	6.002	89.864	1.650	0.054	–
s43	SNG to dehydration	321.57	32.0	20.59	1.000	2.576	0.318	95.299	1.749	0.057	–
s42	V4 condensate	21.66	32.0	20.59	0.000	–	99.943	0.041	0.015	–	–
s38	Water to purification	680.70	40.7	20.59	0.000	0.004	99.934	0.032	0.030	–	–

References

1. Intergovernmental Panel on Climate Change (IPCC). *Climate Change 2022—Mitigation of Climate Change*; IPCC: Geneva, Switzerland, 2022.
2. IEA (International Energy Agency). *World Energy Outlook*; IEA: Paris, France, 2025.
3. *Directive (EU) 2023/2413 of the European Parliament and of the Council of 18 October 2023*; Off. J. Eur. Union 2023, L 2023/2413; Publications Office of the European Union: Luxembourg, 2023.
4. European Biogas Association. *Mapping-e-Methane-Plants-and-Technologies*; EBA: Brussels, Belgium, 2024.
5. *Commission Delegated Regulation (EU) 2023/1184*; 2023.
6. Secretaría de Estado de Energía. *Hoja de Ruta Del Biogás*; Ministerio para la Transición Ecológica y el Reto Demográfico: Madrid, Spain, 2022.
7. *Geopolitics of the Energy Transformation: The Hydrogen Factor*; International Renewable Energy Agency: Abu Dhabi, United Arab Emirates, 2022.
8. International Renewable Energy Agency. *Renewable Power Generation Costs in 2025*; International Renewable Energy Agency: Abu Dhabi, United Arab Emirates, 2026.
9. Red Eléctrica de España (REE). *Informe del Sistema Eléctrico: Informe Resumen de Energías Renovables 2025*; 2026.
10. European Environment Agency. Greenhouse Gas Emission Intensity of Electricity Generation, Country Level. Available online: https://www.eea.europa.eu/en/analysis/indicators/greenhouse-gas-emission-intensity-of-1/greenhouse-gas-emission-intensity-of-electricity-generation (accessed on 9 July 2026).

11. Daniarta, S.; Sowa, D.; Błasiak, P.; Imre, A.R.; Kolasiński, P. Techno-Economic Survey of Enhancing Power-to-Methane Efficiency via Waste Heat Recovery from Electrolysis and Biomethanation. *Renew. Sustain. Energy Rev.* **2024**, *194*, 114301.
12. Tommasi, M.; Degerli, S.N.; Ramis, G.; Rossetti, I. Advancements in CO_2 Methanation: A Comprehensive Review of Catalysis, Reactor Design and Process Optimization. *Chem. Eng. Res. Des.* **2024**, *201*, 457–482. https://doi.org/10.1016/j.cherd.2023.11.060.
13. Ren, J.; Lou, H.; Xu, N.; Zeng, F.; Pei, G.; Wang, Z. Methanation of CO/CO_2 for Power to Methane Process: Fundamentals, Status, and Perspectives. *J. Energy Chem.* **2023**, *80*, 182–206. https://doi.org/10.1016/j.jechem.2023.01.034.
14. Bailera, M.; Lisbona, P.; Romeo, L.M.; Espatolero, S. Power to Gas Projects Review: Lab, Pilot and Demo Plants for Storing Renewable Energy and CO_2. *Renew. Sustain. Energy Rev.* **2017**, *69*, 292–312. https://doi.org/10.1016/j.rser.2016.11.130.
15. Xu, J.; Froment, G.F. Methane Steam Reforming, Methanation and Water-Gas Shift: 1. Intrinsic Kinetics. *AIChE J.* **1989**, *35*, 88–96. https://doi.org/10.1002/aic.690350109.
16. Bremer, J.; Sundmacher, K. Operation Range Extension via Hot-Spot Control for Catalytic CO_2 Methanation Reactors. *React. Chem. Eng.* **2019**, *4*, 1019–1037. https://doi.org/10.1039/c9re00147f.
17. Schlereth, D.; Hinrichsen, O. A Fixed-Bed Reactor Modeling Study on the Methanation of CO_2. *Chem. Eng. Res. Des.* **2014**, *92*, 702–712. https://doi.org/10.1016/j.cherd.2013.11.014.
18. Rönsch, S.; Schneider, J.; Matthischke, S.; Schlüter, M.; Götz, M.; Lefebvre, J.; Prabhakaran, P.; Bajohr, S. Review on Methanation—From Fundamentals to Current Projects. *Fuel* **2016**, *166*, 276–296. https://doi.org/10.1016/J.FUEL.2015.10.111.
19. Gorre, J.; Ortloff, F.; van Leeuwen, C. Production Costs for Synthetic Methane in 2030 and 2050 of an Optimized Power-to-Gas Plant with Intermediate Hydrogen Storage. *Appl. Energy* **2019**, *253*, 113594. https://doi.org/10.1016/j.apenergy.2019.113594.
20. Peters, R.; Baltruweit, M.; Grube, T.; Samsun, R.C.; Stolten, D. A Techno Economic Analysis of the Power to Gas Route. *J. CO_2 Util.* **2019**, *34*, 616–634. https://doi.org/10.1016/j.jcou.2019.07.009.
21. Al-Breiki, M.; Bicer, Y. Techno-Economic Evaluation of a Power-to-Methane Plant: Levelized Cost of Methane, Financial Performance Metrics, and Sensitivity Analysis. *Chem. Eng. J.* **2023**, *471*, 144725. https://doi.org/10.1016/j.cej.2023.144725.
22. Barón, C.; Gómez, L.; Martínez, I.; Bailera, M. Techno-Economic Assessment of the Sorption Enhanced Methanation: Levelized Cost of Methane, Performance Indicators and Sensitivity Analysis. *Int. J. Hydrogen Energy* **2026**, *231*, 154958. https://doi.org/10.1016/j.ijhydene.2026.154958.
23. Gantenbein, A.; Kröcher, O.; Biollaz, S.M.A.; Schildhauer, T.J. Techno-Economic Evaluation of Biological and Fluidised-Bed Based Methanation Process Chains for Grid-Ready Biomethane Production. *Front. Energy Res.* **2022**, *9*, 775259. https://doi.org/10.3389/fenrg.2021.775259.
24. Janke, L.; Ruoss, F.; Hahn, A.; Weinrich, S.; Nordberg, Å. Modelling Synthetic Methane Production for Decarbonising Public Transport Buses: A Techno-Economic Assessment of an Integrated Power-to-Gas Concept for Urban Biogas Plants. *Energy Convers. Manag.* **2022**, *259*, 115574. https://doi.org/10.1016/j.enconman.2022.115574.
25. Yilmaz, H.Ü.; Kimbrough, S.O.; van Dinther, C.; Keles, D. Power-to-Gas: Decarbonization of the European Electricity System with Synthetic Methane. *Appl. Energy* **2022**, *323*, 119538. https://doi.org/10.1016/j.apenergy.2022.119538.
26. Kumar, P.; Date, A.; Shabani, B. Towards Self-Water-Sufficient Renewable Hydrogen Power Supply Systems by Utilising Electrolyser and Fuel Cell Waste Heat. *Int. J. Hydrogen Energy* **2025**, *137*, 380–396. https://doi.org/10.1016/j.ijhydene.2025.05.124.
27. Traisak, O.; Kumar, P.; Das, R.K.; Vahaji, S.; Zhang, Y.; Velankar, V.; Date, A. Integrated Thermoelectric Power Generation and Membrane-Based Water Desalination Using Low-Grade Thermal Energy. *Energies* **2026**, *19*, 1054. https://doi.org/10.3390/en19041054.
28. Chauvy, R.; Dubois, L.; Lybaert, P.; Thomas, D.; De Weireld, G. Production of Synthetic Natural Gas from Industrial Carbon Dioxide. *Appl. Energy* **2020**, *260*, 114249. https://doi.org/10.1016/j.apenergy.2019.114249.
29. Ministerio para la Transición Ecológica y el Reto Demográfico. *Orden TED/181/2025, de 13 de Febrero, por la que se Aprueban las Normas de Gestión Técnica del Sistema Gasista de Competencia Ministerial*; Agencia Estatal Boletín Oficial del Estado: Madrid, Spain, 2025; pp. 27093–27245.
30. Jefatura del Estado. Ley 34/1998, de 7 de octubre, del sector de hidrocarburos; Agencia Estatal Boletín Oficial del Estado: Madrid, Spain, 1998; pp. 33517–33549.
31. Espinosa-López, M.; Darras, C.; Poggi, P.; Glises, R.; Baucour, P.; Rakotondrainibe, A.; Besse, S.; Serre-Combe, P. Modelling and Experimental Validation of a 46 kW PEM High Pressure Water Electrolyzer. *Renew. Energy* **2018**, *119*, 160–173. https://doi.org/10.1016/j.renene.2017.11.081.
32. Biaku, C.Y.; Dale, N.V.; Mann, M.D.; Salehfar, H.; Peters, A.J.; Han, T. A Semiempirical Study of the Temperature Dependence of the Anode Charge Transfer Coefficient of a 6 kW PEM Electrolyzer. *Int. J. Hydrogen Energy* **2008**, *33*, 4247–4254. https://doi.org/10.1016/j.ijhydene.2008.06.006.

33. Webster, J.; Bode, C. Implementation of a Non-Discretized Multiphysics PEM Electrolyzer Model in Modelica. In *Proceedings of the 13th International Modelica Conference, Regensburg, Germany, 4–6 March 2019*; Linköing University Electronic Press: Linköping, Sweden, 2019; Volume 157, pp. 833–840.
34. Bessarabov, D.G.; Wang, H.; Li, H.; Zhao, N. (Eds.) *PEM Electrolysis for Hydrogen Production*; CRC Press: Boca Raton, FL, USA, 2016.
35. Bailera, M.; Lisbona, P.; Peña, B.; Alarcón, A.; Guilera, J.; Perpiñán, J.; Romeo, L.M. Synthetic Natural Gas Production in a 1 kW Reactor Using Ni–Ce/Al_2O_3 and Ru–Ce/Al_2O_3: Kinetics, Catalyst Degradation and Process Design. *Energy* **2022**, *256*, 124720. https://doi.org/10.1016/j.energy.2022.124720.
36. Held, M.; Schollenberger, D.; Sauerschell, S.; Bajohr, S.; Kolb, T. Power-to-Gas: CO_2 Methanation Concepts for SNG Production at the Engler-Bunte-Institut. *Chem. Ing. Tech.* **2020**, *92*, 595–602. https://doi.org/10.1002/cite.201900181.
37. Sanz-Monreal, P.; Mercader, V.D.; Aragüés-Aldea, P.; Durán, P.; Francés, E.; Herguido, J.; Peña, J.A. Techno-Economic Assessment of a Plant for the Upgrading of MSW Biogas to Synthetic Natural Gas by Thermocatalytic Methanation. *Biomass Bioenergy* **2025**, *198*, 107871. https://doi.org/10.1016/j.biombioe.2025.107871.
38. National Renewable Energy Laboratory. *System Advisor Model Version 2017.1.17 (SAM 2017.1.17)*; National Renewable Energy Laboratory: Golden, CO, USA, 2017.
39. Sengupta, M.; Xie, Y.; Lopez, A.; Habte, A.; Maclaurin, G.; Shelby, J. The National Solar Radiation Data Base (NSRDB). *Renew. Sustain. Energy Rev.* **2018**, *89*, 51–60.
40. U.S. Department of Energy (DOE). Technical Targets for Proton Exchange Membrane Electrolysis. Available online: https://www.energy.gov/cmei/fuels/technical-targets-proton-exchange-membrane-electrolysis (accessed on 27 September 2026).
41. IRENA. *Green Hydrogen Cost Reduction*; IRENA: Abu Dhabi, United Arab Emirates, 2020.
42. Dannesboe, C.; Hansen, J.B.; Johannsen, I. Catalytic Methanation of CO_2 in Biogas: Experimental Results from a Reactor at Full Scale. *React. Chem. Eng.* **2020**, *5*, 183–189. https://doi.org/10.1039/c9re00351g.
43. Turton, R.; Shaeiwitz, J.A.; Bhattacharyya, D.; Whiting, W.B. *Analysis, Synthesis, and Design of Chemical Processes*, 5th ed.; International Series in the Physical and Chemical Engineering Sciences; Pearson: Boston, MA, USA, 2018.
44. Woods, D.R. Appendix D: Capital Cost Guidelines. In *Rules of Thumb in Engineering Practice*; Wiley: Hoboken, NJ, USA, 2007; pp. 376–436.
45. Andreasen, A.; Bonto, M.; Montero, F. A Framework for Optimisation and Techno-Economic Analysis of CO_2 Pressurisation Strategies for Pipeline Transportation. *Sci. Technol. Energy Transit.* **2025**, *80*, 18. https://doi.org/10.2516/stet/2024109.
46. International Renewable Energy Agency (IRENA). *Renewable Power Generation Costs in 2023*; IRENA: Abu Dhabi, United Arab Emirates, 2024.
47. Ademollo, A.; Calabrese, M.; Carcasci, C.; Joshi, I.; Vaccaro, M. Comparative Techno-Economic Assessment of Stationary Hydrogen Storage Technologies. *Int. J. Hydrogen Energy* **2026**, *199*, 152849. https://doi.org/10.1016/j.ijhydene.2025.152849.
48. Cornot-Gandolphe, S. *The European Biomethane Sector at a Critical Juncture: Stronger Policy Alignment Will Matter*; IFRI: Paris, France, 2026.
49. *Informe Anual del Mercado Ibérico del Gas 2025*; MIBGAS: Madrid, Spain, 2026.

Disclaimer/Publisher's Note: The statements, opinions and data contained in all publications are solely those of the individual author(s) and contributor(s) and not of MDPI and/or the editor(s). MDPI and/or the editor(s) disclaim responsibility for any injury to people or property resulting from any ideas, methods, instructions or products referred to in the content.